

Article

A Comprehensive Review on Seismocardiogram: Current Advancements on Acquisition, Annotation, and Applications

Deepak Rai ¹, Hiren Kumar Thakkar ^{2,*}, Shyam Singh Rajput ¹, Jose Santamaria ^{3,*}, Chintan Bhatt ⁴
and Francisco Roca ⁵

¹ Department of Computer Science and Engineering, National Institute of Technology Patna, Patna 800005, India; ramdeepakniwash@gmail.com (D.R.); shyam.rajput.cs@nitp.ac.in (S.S.R.)

² Department of Computer Science and Engineering, School of Engineering and Sciences, SRM University, Andhra Pradesh 522240, India

³ Department of Computer Science, University of Jaén, 23071 Jaén, Spain

⁴ U & P U. Patel Department of Computer Engineering, CSPIT, Charotar University of Science and Technology (CHARUSAT), Anand 388421, India; chintanbhatt.ce@charusat.ac.in

⁵ Department of Mathematics, University of Jaén, 23071 Jaén, Spain; froca@ujaen.es

* Correspondence: hirenkumar.t@srmmap.edu.in (H.K.T.); jslopez@ujaen.es (J.S.)

Abstract: In recent years, cardiovascular diseases are on the rise, and they entail enormous health burdens on global economies. Cardiac vibrations yield a wide and rich spectrum of essential information regarding the functioning of the heart, and thus it is necessary to take advantage of this data to better monitor cardiac health by way of prevention in early stages. Specifically, seismocardiography (SCG) is a noninvasive technique that can record cardiac vibrations by using new cutting-edge devices as accelerometers. Therefore, providing new and reliable data regarding advancements in the field of SCG, i.e., new devices and tools, is necessary to outperform the current understanding of the State-of-the-Art (SoTA). This paper reviews the SoTA on SCG and concentrates on three critical aspects of the SCG approach, i.e., on the acquisition, annotation, and its current applications. Moreover, this comprehensive overview also presents a detailed summary of recent advancements in SCG, such as the adoption of new techniques based on the artificial intelligence field, e.g., machine learning, deep learning, artificial neural networks, and fuzzy logic. Finally, a discussion on the open issues and future investigations regarding the topic is included.

Keywords: cardiovascular; seismocardiography (SCG); noninvasive; SCG annotation; SCG acquisition; SCG applications; artificial intelligence; machine learning; deep learning



Citation: Rai, D.; Thakkar, H.K.; Rajput, S.S.; Santamaria, J.; Bhatt, C.; Roca, F. A Comprehensive Review on Seismocardiogram: Current Advancements on Acquisition, Annotation, and Applications. *Mathematics* **2021**, *9*, 2243. <https://doi.org/10.3390/math9182243>

Academic Editors: Maria Laura Manca and Vladimir Simeonov Gueorguiev

Received: 16 August 2021

Accepted: 6 September 2021

Published: 12 September 2021

Publisher's Note: MDPI stays neutral with regard to jurisdictional claims in published maps and institutional affiliations.



Copyright: © 2021 by the authors. Licensee MDPI, Basel, Switzerland. This article is an open access article distributed under the terms and conditions of the Creative Commons Attribution (CC BY) license (<https://creativecommons.org/licenses/by/4.0/>).

1. Introduction

Recently, human cardiac health deteriorated significantly because of several risk factors such as unhealthy lifestyle, physical inactivity, and poor work-life balance [1]. Cardiovascular diseases (CVD) are the principal source of an increasing number of deaths across the globe. According to the latest report published by the American Heart Association (AHA), 24.3 million people over the age of 20 are affected by CVD in the US [2]. Nearly 17.6 million deaths occurred globally due to CVD. An AHA report estimated that more than 130 million, i.e., 45.1% of the US population, will suffer from some form of CVD by 2035. Therefore, cardiac health monitoring became an essential public health goal [3]. Cardiac anomalies occur irregularly and may progress completely unnoticed, which makes it very challenging to detect at an early stage [4]. There are several existing technologies for monitoring cardiac health [5,6]. Several noninvasive monitoring approaches are shown in Figure 1.

Specifically, Phonocardiography (PCG) detects sounds produced by the heart and blood flow [7]. Electrocardiography (ECG) studies the electrical functioning of the heart [8]. Recently, the viability of ECG for cardiac health monitoring was reviewed in [9]. In ballistocardiography (BCG), the mechanical vibrations induced by heart and cardiac reaction

forces acting on the whole body are measured ([10]). Next, impedance cardiography (ICG) was proposed to measure the changes in thoracic impedance induced due to changes in the fluid content of the chest [11]. Echocardiography (ECHO) is a cardiac imaging method based on ultrasound [12]. SCG studies mechanical vibrations induced by heart, which, unlike BCG, measures only cardiac reaction forces acting locally on the chest [13]. In the early seventies, nuclear cardiology (NC) was introduced as a method where radioisotopes are injected into the vascular system, and the emitted radiation is recorded externally [14]. As a subsequent improvement, the X-ray computed tomography (X-CT) approach is an imaging modality where slice images of the heart are created using X-rays [15]. Next, cardiovascular magnetic resonance imaging (C-MRI) is a cardiac imaging method based on nuclear magnetic resonance [16]. Few years back in 2016, Gyrocardiography (GCG), a noninvasive technique based on SCG was proposed. It assesses the cardiac motion using gyroscope—a sensor that measures the angular motion [17,18]. The techniques mentioned above are reliable but they provide very little knowledge of more complex cardiac activities. Among them, SCG is one such technique that facilitates the monitoring of cardiac mechanical activities. However, due to technological limitations and several competing methods, SCG did not gain widespread clinical use in the past. Nevertheless, the development of modern technologies recently brought interest back to SCG. Additionally, compared to that of existing cardiac methods, SCG can provide a cost-effective solution with the added advantage of regular and automated monitoring.

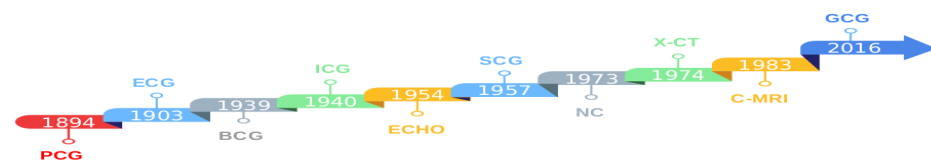


Figure 1. Timeline evolution of existing techniques for monitoring cardiac health.

As stated, SCG is a noninvasive measurement of cardiac vibrations transmitted to the chest wall due to the heart's mechanical activities [19]. In 1959, it was observed in [20] that the influence of heart sound nearly disappears at low frequencies, which makes it difficult to interpret its correlation with cardiac functions. Therefore, further study was required to confirm the use of heart sounds for diagnosis and cardiac function evaluation. After a period of nearly 26 years, SCG was reintroduced in 1990 in USA to monitor cardiac vibrations [19]. The recordings were correlated with acute and chronic changes in the functioning of left-ventricular (LV) [21]. In 1994, the combination of SCG and ECHO was also evaluated [22], and the low-frequency cardiac vibrations became a promising niche of research. However, considering the advancement of ECG and other medical imaging techniques, SCG was again largely abandoned throughout the 90s. It was after the emergence of micro electromechanical system technology that research interest in SCG returned [23]. In particular, SCG and BCG are the only two techniques that cover both aspects, i.e., the myocardial vibrations produced by cardiac muscle contraction and the vibrations caused due to arterial circulation resulting from the flow of blood [24].

Nowadays, there is an increasing interest in the adoption of SCG-based noninvasive assessment as an approach for monitoring cardiac health. Significant advancements in lightweight sensor technology made SCG resurgent, and it opened a new perspective for its clinical and in-home use. Existing reviews on SCG mainly concentrate on advances in instrumentation and signal processing [25,26]. Although SCG was thoroughly investigated in the last few years, it requires a comprehensive and updated review of its three most critical regarding: acquisition, annotation, and current applications.

In this paper, our contribution is two-fold: (i) review and taxonomy of the current SCG acquisition and annotation approaches in the SoTA, and (ii) an overview of the recent application approaches in SCG.

The rest of the paper is organized as follows. Section 2 discusses data acquisition. Next, Section 3 describes data preprocessing and noise reduction schemes. Sections 4 and 5

discusses the annotation of signal feature points and introduce some recent works in the field of SCG. Section 6 is aimed at testing the inherent properties of using SCG signals by performing several demonstrative experiments. Sections 7 and 8 describe novel applications and present several open challenges to be addressed in future investigations. Finally, Section 9 concludes this paper with the outcomes achieved in this research.

2. Data Acquisition

SCG signals are mostly composed of very low-frequency waves, which are much below the human hearing capacity [27]. Due to low auditory sensitivity, it is very difficult to accurately extract the signal characteristics. Hence, an efficient and robust acquisition system for extracting SCG signals is required.

Acquisition of SCG signals is divided into two categories, i.e., contact- and noncontact-based methods. In the former methods, the sensors or the acquisition device is physically attached to the body of the patient which is sometimes uncomfortable for the subject and requires some experience from the practitioner. However, the latter methods have no such issues, and they have the potential to acquire signals without physically attaching the device to the body. The overall taxonomy of the SCG acquisition task is shown in Figure 2.

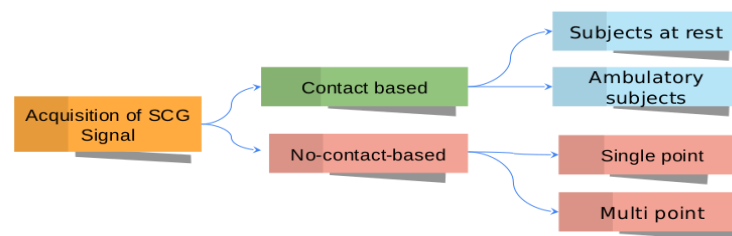


Figure 2. Taxonomy of the SCG acquisition task.

The next subsections are devoted to introducing the SCG data acquisition approaches that were frequently adopted in the SoTA.

2.1. Contact-Based Acquisition from Patients at Rest

In [28], a simplified model was proposed to explain the mechanical coupling of the 3-axis accelerometer, gyroscope, and chest wall. Gyroscope was used in parallel to accelerometer because rotational components of chest wall vibrations induced by cardiac mechanical activities may provide better insights for cardiac activities. Then, the author also used a hardware setup as shown in Figure 3, which consists of a wireless sensor node positioned to the middle of the sternum near the 3rd rib and attached with a tightened strap on the front chest wall of the patient.

Specifically, the sensor node consists of a 3-axis MEMS accelerometer (Kionix KXR5-2042, Kionix Inc, Ithaca, NY, USA) and a 3-axis MEMS gyroscope (Invensense MPU9150, Invensense Inc, Sunnyvale, CA, USA). Both accelerometer and gyroscope make use of the same coordinate system. Additionally, Z-axis represents the dorsal-ventral direction, which corresponds to the linear acceleration reading of SCG. On the other hand, both the X-axis and the Y-axis represent the head-to-foot direction and shoulder-to-shoulder direction, respectively, which correspond to the angular speeds. In [29], a wireless acquisition system was developed that was comprised of high-resolution time-based MEMS accelerometer capable of achieving micro-g resolutions. Time-based accelerometers are more accurate compared to that of the conventional capacitive accelerometers. The acquisition system introduced in the proposed work contained a small system measuring $40 \times 40 \times 20 \text{ mm}^3$ having wireless capabilities, as shown by the block diagram in Figure 4.

The proposed system included a differential actuation mechanism and an application-specific integrated circuit (ASIC) for accelerometer operation control. Three main sub-systems were used: the ASIC controller, the ECG signal acquisition circuit, and the Programmable System on Chip (PSoC). ASIC controls the MEMS element through a digital-

to-analog converter. The ECG acquisition system was based on AD8232 (Analog Devices, Norwood, MA, USA), connected through an analog-to-digital converter that allowed the reading of a single-lead ECG. The PSoC (Cypress Semiconductor Corporation, San Jos, CA, USA) is aimed at reading the signal data, synchronizing it, and transmitting the same over the integrated blue-tooth, low-energy peripheral.

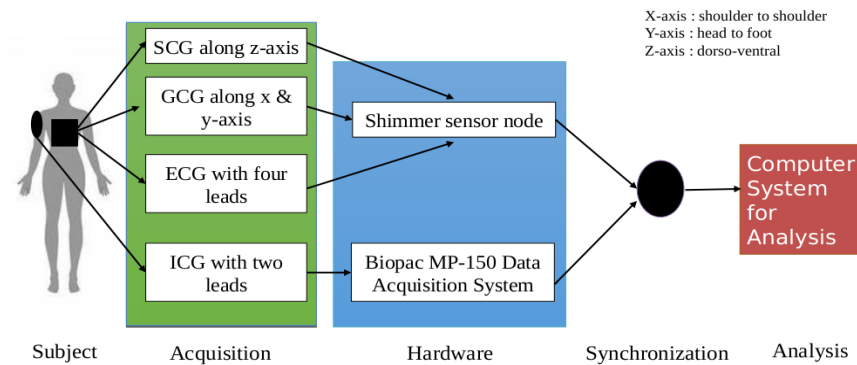


Figure 3. SCG contact-based hardware setup containing accelerometer and gyroscope.

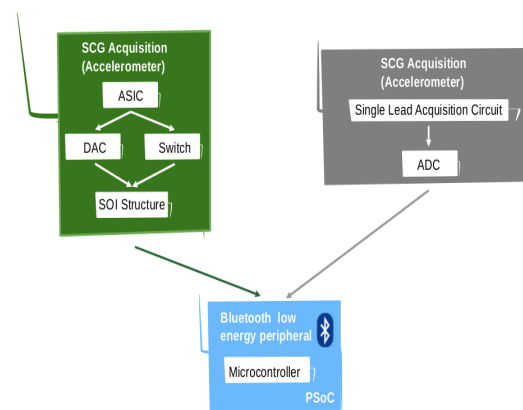


Figure 4. Block diagram of SCG contact-based acquisition device.

The development of novel information and communication technologies in the field of health care services encouraged and facilitated the research in mobile health (m Health). In [30], an early warning system was proposed for regularly monitoring cardiac health. The designed system consisted of three different modules: (i) data acquisition module; (ii) data communication module, and (iii) an early warning module. The data acquisition process was accomplished using a body area network-based by fitting various sensors to specific parts of the body. The data acquisition module was designed in such a way that the data collection process was not specific to the laboratory. It could collect data round the clock using small and energy-efficient wireless body sensors. However, directly fitting the sensors on the body surface of the patient was reportedly uncomfortable. Recently, in [31] a novel and convenient electro-mechano-acoustic cardiovascular (EMAC) sensing tattoo was designed by integrating the soft SCG sensor by means of a pair of soft gold ECG electrodes. Then, the EMAC tattoo could perform synchronous ECG and SCG measurements. Some other popular existing wearables for collecting different cardiac data are smart belt, smart band, smart helmet, and smart cloth, which may be enhanced for collection of SCG data.

In [32], a body area network-based wireless sensing system, i.e., KNOWME, was designed. It used accelerometer, oximeter, and electrocardiograph sensors for regularly monitoring and analyzing signals through smartphones. In [33], a body area network-based sensor was designed to simultaneously collect the ECG and SCG signals. The model contained separate ECG and SCG sensing modules as shown in Figure 5.

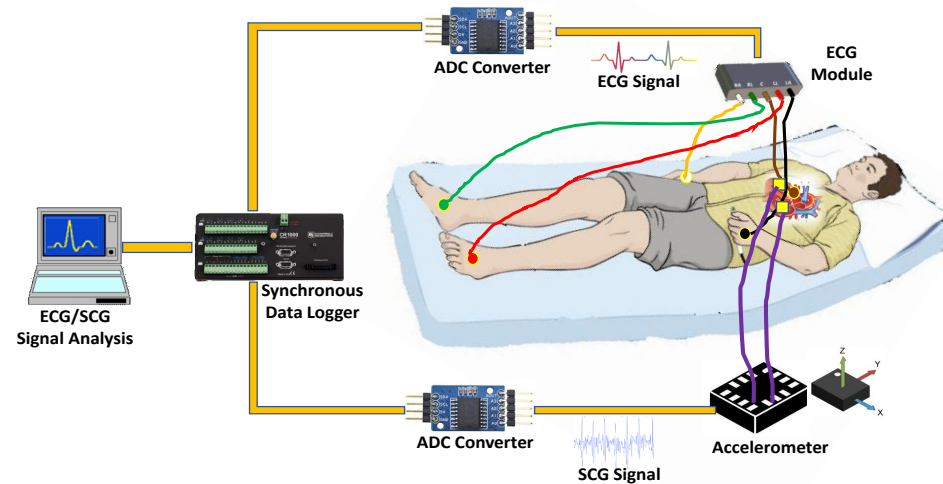


Figure 5. Architecture of ECG/SCG data collection model.

The SCG sensing module was placed at the tricuspid valve (TV) and the ECG sensing module (i.e., the electrode) was placed at the right arm. For ECG sensing, high-quality disposable electrodes from bio-medical instruments (Clinton Township, MI, USA) were used. On the other hand, the accelerometer sensor LIS331DLH (ST microelectronics, Geneva, Switzerland) was used for SCG sensing. The sensing ability, sensing range, and gravitational force sensitivity of the SCG sensing module was set to 0.5 Hz to 1 kHz, +2 g to −2 g, and 1 mg, respectively. The bandpass filter with frequency 0.5–50 Hz and sampling rate 1000 Hz was applied to get the required ECG and SCG signals. Micro-controller system ADuC7020 (Analog devices Inc., Cambridge, MA, USA) was used for communication between ECG/SCG sensing modules to the analog-to-digital converter. Finally, a 16/35 system (AD instruments, Dunedin, New Zealand) was used for synchronous data logger Power Lab to further amplify and filter the concurrent signals.

2.2. Contact-Based Acquisition from Ambulatory Patients

A major challenge in the acquisition of SCG and other cardio mechanical signals is that high-fidelity signals can only be obtained at rest position. Any type of movement like walking will reduce the signal-to-noise ratio and can even make the signals unreadable. That is why most of the researchers are prone to use wearable sensing of cardio-mechanical signals at rest state only. Recently, in [34] it was shown that sensing during movement can provide deeper insight into cardiovascular functions. A small wearable patch (See Figure 6) was developed for simultaneously measuring ECG and SCG signals during walking at different speeds.

The patch recorded data onto a micro secure digital (Micro-SD) card and the patch contained ATMEGA1284P micro-controller (Atmel Corporation, San Jose, CA, USA). For ECG sensing, an analog-front-integrated circuit with an on-board analog-to-digital converter ADS1291 (Texas Instruments, Dallas, TX, USA) was used. Micro-USB was an optional addition for debugging or telemetry (i.e., remote monitoring) [35]. Last, an accelerometer BMA280 (Bosch Sensortec GmbH, Reutlingen, Germany) was used for SCG sensing. All the signals were sampled at 1 kHz.

2.3. Noncontact Based Acquisition from Single Point

A noncontact method based on laser doppler vibrometry (LDV) was proposed for measuring the chest wall vibrations. This enabled the possibility of detecting SCG features. However, LDV suffers from some major hindrances like cost, size, and its inability to penetrate through obstacles [36]. Later, this inability of penetrating through obstacles was well-considered, and microwave signals were used, which can penetrate through many solid objects. In [37], a microwave doppler radar-based contactless technique for acquiring SCG signals was proposed; the technique was able to collect valuable mechanical aspects

of cardiac health. However, cardiac induced vibrations measured through the proposed technique also contained respiration patterns in addition to a heartbeat. This was dealt with by applying order 10 comb filters with a bandwidth of 0.024 Hz to eliminate the interference caused by up to 10th order respiration harmonics. In [38], another microwave doppler radar-based sensing of the SCG signal was proposed. A system was set up to capture the radar acceleration waveforms (RAW). The setup mainly comprised of four components: microwave signal generator N5222A (Agilent), horn antennas A-INFO LB20180-SF, I/Q frequency downconverter HMC951LP4E (Hittite), and data acquisition unit AD7770 (Analog Devices). In parallel contact, the SCG sensor was used to acquire the SCG signal and the similarity between both RAW and SCG was compared; there was a high morphological similarity between both RAW and SCG.

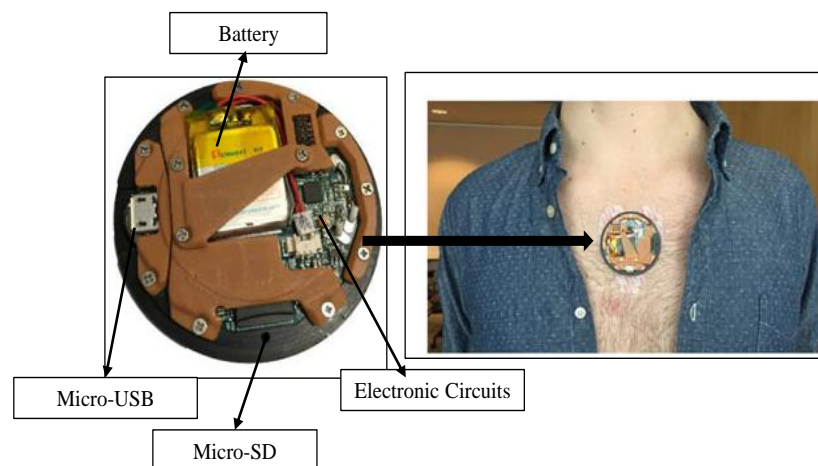


Figure 6. A wearable device for the collection of ECG/SCG signals and its placement.

2.4. Noncontact-Based Acquisition from Multipoint

One primary limitation of the noncontact sensing methods discussed in the literature is that they are mostly confined to single point measurement. Recently, in [39] a system namely ICARE (Cardio Respiratory Imager) was developed, which allows us to study the complete thoracic and abdominal systems simultaneously. ICARE can detect surface motion of any region of interest. The system consisted of a 3D airborne noncontact ultrasound vibrometer, which was composed of three emission arrays arranged vertically and one 16×16 square array of receivers (Knowles microphone FG-23629) in the middle. A total of 32 transducers (Murata MA40S4S) were uniformly distributed over each panel of 24×24 cm². The panel in the middle combines both the radiating and receiving elements (32 emitting transducers and 256 microphone receivers). For a visual representation of the subject, a camera was also included in the system. The ICARE system works in pulse-echo mode. Emitters were connected to a programmable digital-to-analog acquisition card with 32 channels (D-TACQ ACQ1001). Each of the 32 channels was connected to 3 transducers—one for each emission panel. The emission waveform was a linearly modulated frequency signal, which ranges from 35–45 kHz. The time duration was 320 μ s. The signals were successively emitted by the 32×3 emitting transducers with a time delay of 160 μ s between 2 signal emissions. The total duration of 1 sequence of emission was 5.12 ms, and the repetition rate was 195 Hz. Receivers were connected to a 256-channel analog-to-digital acquisition card ACQ196 (DAQ D-TACQ 16 bits, 400 kS/s). Finally, a comparison of various SCG acquisition techniques is presented in Table 1.

Table 1. Comparison of SCG acquisition techniques.

Type	Subject Position	Methodology	Acquisition Device	Sampling Rate	Location of Device	Details of Subjects	Limitation
Contact based	Siting	Gyroscope was used in parallel with accelerometer for recording rotational component of the cardiac signal [28].	3-axis accelerometer (Kionix KXR85-2042) and 3-axis gyroscope (Invensense MPU9150)	256 Hz	Near to 3rd rib on sternum	5 (3 male + 2 female), all healthy	Proposed method is not feasible for a large number of subjects, including elderly and unhealthy subjects.
	Supine	High resolution time based accelerometer was used [29].	MEMS accelerometer	248 Hz	Near to heart on sternum	22 (16 male + 6 female), 5 healthy, 17 CVD patient	Proposed method is not validated against any standard benchmark signal. Proposed method is not feasible in real life as it did not work for subjects with psychological factors like nervousness, excitement etc.
	Supine	Multichannel acquisition of signal was done by placing sensors at 4 different valvular auscultation positions [30].	Accelerometer (ST Microelectronics LIS331DLH)	400 Hz	At tricuspid, mitral, pulmonary, and aortic valve	50 (25 male + 25 female), 20 healthy, 30 unhealthy	Only basic features are considered. One lead ECG signal was used.
	Supine	Sensor placed only at tricuspid valve because inter ventricular septum is located beneath it which provide more clear signal [33]	Accelerometer (ST Microelectronics LIS331DLH)	1000 Hz	At tricuspid valve	20 (10 male + 10 female), 12 healthy, 8 unhealthy	Proposed technique is not suitable for elderly and CVD-affected subjects. It does also not work in real-life, as for majority of the time, the walking surface for any subject is not smooth and level.
	Walking	Used wearable patch for acquiring from ambulatory subjects [34].	Accelerometer (Bosch Sensortec BMA280) fitted in a patch	1000 Hz	On sternum	17 (11 male + 6 female), All healthy	
Noncontact-based	Supine	Optical recording of the movements of the chest wall was done by means of laser doppler vibrometry [36].	Laser vibrometer	N/A	Laser head placed at 1.5 m from the subject chest wall	10 (5 male + 5 female), All healthy	Proposed technique is very expensive because of laser vibrometer.
	Siting	Microwave radar based technique used for recording accelerations [38].	Microwave signal generator, horn antennas and I/Q frequency down converter	N/A	50 cm from the subject	8 (all male), All healthy	Proposed setup is not able to cover any specific location on the torso area of the subject. Only the area under radar antenna is covered.
	Siting	3D SCG images with high frequency frame rate obtained using ultrasonic imaging technique [37].	3D airborne noncontact ultrasound vibrometer and camera	N/A	In front of subject at 72 cm distance	8 (all male), All healthy	Proposed method assumes that the sternum moves as a single solid object.

3. Data Preprocessing and Noise Reduction

The SCG signals acquired through accelerometer need to be preprocessed to transform the raw signal into a clean signal that is more suitable for further analysis and is easily interpretable by humans. In the case of SCG signals, preprocessing generally refers to noise removal from the raw signal for getting closer to the actual SCG signal. There are various reasons why preprocessing is required for SCG signals; most of the time, SCG signals get adulterated by noise from various sources including motion artifacts, environmental vibrations, and sensor mechano-electronics. This signal adulteration might cause errors in feature extraction, which can lead to wrong signal classification. When the patient is moving, the motion artifact recorded by the accelerometer is stronger than the actual heart-induced vibration signals at the chest wall. It becomes tough to identify the peaks in the SCG signals. SCG signal preprocessing is still an active area of research, though there is no such globally accepted technique. Researchers are free to choose how to transform the raw signal.

In the past, most researchers applied conventional band-pass filters for removing baseline wandering, body movements, and breathing artifacts from SCG signals. In [34], finite impulse response filters were used for bandpass filtering, having the following cutoff frequencies: 0.8–40 Hz for the ECG, and 0.8–35 Hz for SCG signals. After getting the filtered signal, they were segmented into individual frames. The collected extracted frames were called an ensemble. The obtained ensembles were averaged to get signals with reduced noise. For correcting the baseline wandering, high-frequency components of the acquired signal were removed. The signals obtained from the initial measurement unit discussed in [40] were filtered using a band-pass filter with cut-off frequency 0.8–25 Hz. In [41], infinite impulse response Butterworth filters were used as band-pass filters with cutoff frequency 0.8–25 Hz for filtering the SCG signals.

In [42], eighth-order Bessel low pass filter was used for the antialiasing of the signals generated by the accelerometer. The filter was set to the cutoff frequency of 100 Hz and attenuation of at least 96 dB at 800 Hz. All signals were band-pass filtered within a range of 0.5–40 Hz frequency. In [43], a method for analyzing nonlinear and nonstationary data was developed based on empirical mode decomposition (EMD), an adaptive time-frequency data analysis method. EMD is very versatile for the extraction of signals generated from noisy nonlinear and nonstationary processes. A real-time approach for detecting the motion and noise (MN) artifacts were proposed for cardiac signal collected from Holter monitors. The approach used EMD for obtaining the first-order intrinsic mode function (F-IMF) for isolating the high-frequency components of the signal under the assumption that they contain most of the MN artifacts. Then, the high-pass-filtered signal was looked-up for signatures of randomness associated with MN artifacts. The methods utilized were Shannon entropy, mean, and variance values. A threshold value was calculated based on the study of 15 healthy patients with 24-h Holter recordings. A threshold was used for separating the clean and MN-corrupted data.

In [44], an ensemble empirical mode decomposition (EEMD) based filter was proposed for noise removal from vibrocardiographic (VCG) signals. The VCG signals were first decomposed into a set of intrinsic mode functions (IMF), and then the partial sum of IMFs was done for removing the white noise. In [45], to evaluate the capability of EEMD-based filter in noise cancellation, white Gaussian noise was added to pollute the VCG signal, with the signal-to-noise ratio (SNR) ranging from 1–20 dB.

In [46], the effectiveness of EMD-based, EEMD-based, and FIR Wiener filters for removing the Gaussian noise from ECG signals was studied. Researchers mostly used only one accelerometer placed on the sternum. Recently in [47], a multi accelerometers-based noise removal technique was proposed. Accelerometers were placed in various positions on the chest. The combination of all three axes of the accelerometer was also examined to see if a better detection can be obtained rather than using only the z-axis. The study reported that the use of the multiaccelerometer for noise removal outperformed the single-sensor method.

4. Annotation of Signal Feature Points

Annotation helps to achieve a better understanding of the signal by labeling some interesting points known as feature points of the acquired signal. In [22], nine feature points were identified corresponding to the echocardiogram signal. The identified points and their correspondence with echocardiogram signals are shown in Table 2. In our review, we categorized the overall SCG signal annotation process in four different categories: temporal envelope-based with ECG, temporal envelope-based without ECG, machine learning-based, and visual inspection and comparison-based.

4.1. Temporal Envelope-Based with ECG as Reference

In [48], an automated method based on temporal envelope calculation was proposed for annotation of AV Closure (AC) and isovolumic movement (IM) points on the SCG signal with reference to the ECG signal. The high-frequency acceleration (HFACC) signals were used to facilitate the annotation task. Four different envelope calculation methods were used: Cardiac Sound Characteristic Waveform (CSCW), Shannon, Absolute, and Hilbert. The CSCW envelope calculation method produced the highest detection accuracy for both IM and AC. The overall process of detection is shown in Figure 7.

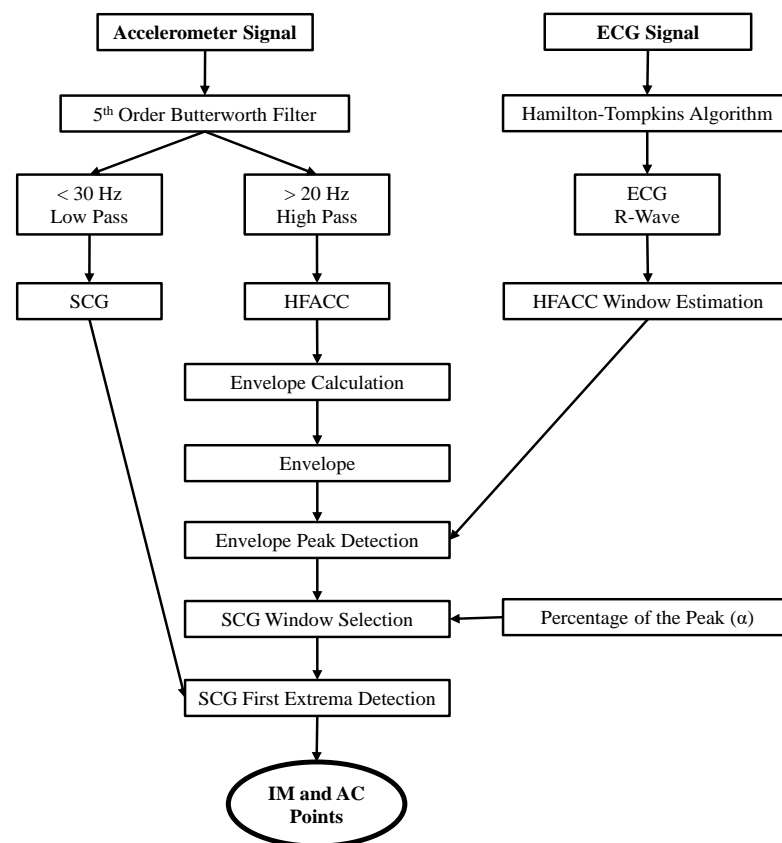


Figure 7. Process of detecting AC and IM Points.

In [49], an automated approach for detecting AO and AC feature points with reference to ECG Q-wave was proposed. The approach was based on the formulation of the initial template by calculating the average of the first few dominant beats in the cardiac cycle and then finding the rough estimate about the location of AO and AC points. Further, finer estimates were obtained by detecting the peaks in the sliding templates calculated by taking averaging the previous values and the incoming value. This approach also helped in minimizing the effects of noise and distortions. In the initial template, the AO peak was identified as the maxima in the interval of $Q + 45$ ms, $Q + 125$ ms, whereas AC peak was identified as the maxima in the interval $AO + 240$ ms, $AO + 350$ ms.

4.2. Temporal Envelope-Based without ECG as Reference

In [50], an algorithm for detecting AO point without ECG R-wave as reference was proposed. The algorithm was based on dominant multiscale kurtosis (DMK) and dominant multiscale central frequency (DMCF) using wavelet. Kurtosis measurement gives the sharpness of the peak of any probability distribution. The multiscale kurtosis gives the estimation of Gaussianity of the signal sub-bands. Kurtosis value equal to 3 represents Gaussian, less than 3 represents sub-Gaussian, and greater than 3 represents super-Gaussian [51]. The central frequency of any signal gives the centroid of the corresponding power spectrum. Multiscale central frequency computes the center of gravity of each signal sub-bands. The sub-bands with DMCF in the frequency range of 6–45 Hz are only considered (i.e., the sub-bands whose central frequency follows the systolic profile). DMK and DMCF together provided criteria for selecting the most probable signal sub-band containing AO peak. The signal was reconstructed and further enhanced with weights based on relative squared dominant multiscale kurtosis (RSDMK). RSDMK was calculated for the selected sub-bands as the normalized sum of the squared DMK. Finally, the envelope was constructed using Shannon energy (SE), and Gaussian derivative filtering based peak detection logic was used for detecting AO point. In [52], a new method based on continuous wavelet transform (CWT) for detecting AO and IM points was proposed. It did not use ECG as the reference signal. CWT was used as the base and approximation was done based on certain decision rules followed by a fine position detection point.

4.3. Machine Learning-Based Approach

In [53], an automatic algorithm was proposed for detecting the specific fiducial points (IM, AO, and AC). The algorithm used two approaches: using ECG as a reference and the other without ECG as a reference signal. In the absence of an ECG signal, the heart rate envelope was used for detection. Unlike in previous contributions, the proposed algorithm used a more accurate window for envelope calculation with the help of moving average filtering. The machine learning-based approach was used for accurate estimation of the specific fiducial points. The probabilistic measure was used to discard the low-quality cardiac cycles.

Recently, in [54], a binary classification-based automatic and fast annotation scheme was proposed. The three different classifiers: Naive Bayes (NB), Logistic Regression (LR), and Support Vector Machine (SVM) were used for annotation. The main objective was to perform the real-time automatic annotation in continuous manner. The complex ML classifiers may not serve this purpose as they require greater computational power and more time for parameter tuning. The NB, SVM, and LR methods were exclusively chosen as they are highly robust against over-fitting, besides being significantly less computer-intensive. Most importantly, the latter three classifiers require few parameters to tune in, which is a suitable feature for achieving fast learning and annotation. An annotation framework was designed, which was divided into three parts: preprocessing, training, and testing. For training purposes, three different features were selected, namely, amplitude, time of appearance, and count. Before testing, the preprocessing of the signals was done to identify the candidate peaks. In the preprocessing phase, three different zones were used for reducing the search area. The maxima and the minima in each zone were identified as the potential candidate peaks. The trained classifiers were finally used for filtering out the undesired candidate peaks and selecting the desired peaks. The models were rigorously validated according to the metrics *Precision*, *Recall*, and *F-measure*, followed by 5-fold cross-validation. The comparative results with the recent state-of-the-art schemes establishes the robustness of the proposed method.

4.4. Visual Inspection and Comparison-Based Approach

In [55], a technique based on visual inspection of echocardiographic images was proposed. The timing of all valvular opening and closing was identified using m-mode echo images. The timing of peak blood flow through each valve was identified using

pulse-wave doppler images. This timing information was simultaneously compared with that of the SCG signal. The technique was able to identify six new feature points: LCV, SCV, AF, PF, MF_A , and MF_E shown in Table 2.

Table 2. SCG feature points.

Feature Point	Physiological Event	Location Identifier on SCG Signal with Reference to ECG
AS	Peak of Atrial Systole	2nd positive peak occurring after ECG P-wave on SCG.
PAI	Peak Atrial Inflow	Point on 1st positive slope after AS on SCG.
MC	Mitral-valve (MV) Closure	Beginning of the sharp downslope on SCG after onset of ECG QRS complex.
IM	Isovolumic Movement	Lowest point of the downslope beginning at MC on SCG.
AO	Aortic-valve (AV) Opening	Peak of the upsloping segment starting at IM on SCG.
PSI	Peak Systolic Inflow	Point on the 2nd positive slope after AO on SCG.
IC	Isotonic Contraction	Lowest point of the downslope beginning at AO on SCG.
RE	Peak of Rapid systolic Ejection	Peak of the rounded positive wave after IC on SCG.
AC	AV Closure	Sharp down-going slope change on SCG near the end of ECG T-wave.
MO	MV Opening	2nd lowest point on the downslope after AC on SCG.
EVF	Early Ventricular Filling	Point on 1st positive slope after MO on SCG.
RF	Peak of Rapid diastolic Filling	2nd rounded peak of the SCG after MO.
LCV	Left ventricular lateral wall contraction peak velocity	Identified by matching the MV trace of SCG with tissue doppler echocardiographic images of LV lateral wall.
SCV	Septal wall contraction peak velocity	Identified by matching the TV trace of SCG with tissue doppler echocardiographic images of interventricular septal wall.
AF	Transaortic valvular peak flow	Identified by matching the AV trace of SCG with pulse-wave doppler echocardiographic images of AV.
PF	Transpulmonary peak flow	Identified by matching the pulmonary valve (PV) trace of SCG with pulse-wave doppler echocardiographic images of PV.
MF_A	Transmitral atrial contraction peak flow	Identified by matching the MV trace of SCG with pulse-wave doppler echocardiographic images.
MF_E	Transmitral ventricular relaxation peak flow	Identified by matching the MV trace of SCG with pulse-wave doppler echocardiographic images.

In [56], a method was proposed to define 8 different fiducial points correlated with different cardiac physiological events identified by ultrasound imaging. SCG signals were manually annotated to ensure uniformity in the way of labeling the points with the same characteristics. A tool in MATLAB was developed for the same purpose. Annotation was done in two steps: firstly, all significant peaks and valleys were marked; secondly, different events were separately labeled in systolic and the diastolic complex. Common patterns were identified for labeling in the systolic and the diastolic complexes. The Pearson's Linear Correlation Coefficient was used for finding the correlation between the fiducial points and the physiological events found in the ultrasound images. After finding the correlation, the mean differences and the standard deviation were calculated between the SCG fiducial points and the corresponding points using the ultrasound images. The combination of the time difference and correlation gave an indication as to which SCG fiducial points best corresponds to which physiological event found in the ultrasound images. The significant outcome of the proposed method was that the physiological events do not always take place at the local extrema of the SCG signal, but it may take place on the slopes of the signal. A total of eight points, namely, AS, PAI, MC, AO, PSI, AC, MO, and EVF, were found as shown in Table 2 with their corresponding physiological events. Table 3 compares the different annotation techniques.

Table 3. Comparison of SCG Annotation techniques.

Type	Methodology	Reference Signal	Feature Points Identified	Characteristics of Patients	Limitations
Envelope-based	Four different envelope calculation methods, namely, CSCW, shannon, absolute, and hilbert, were used and compared [48].	ECG	AC, IM	67 (35 male + 32 female), All healthy; 18(15 male + 3 female), Increased Heart Rate	The proposed technique only considers the high frequency components of the signal.
	Moving average sliding template with initial condition for AO (maxima in interval Q + 45 ms and Q + 125 ms), for AC (maxima in interval AO + 240 ms and AO + 350 ms) [49].	ECG	AO, AC	Four (all male), All healthy	The proposed technique is not feasible in real-life as it only works for the stationary patients. It did not consider the distortion due to motion artifacts.
	Continuous wavelet transform was used with certain decision rules [52].	N/A	AO, IM	20 (12 male + 8 female), All healthy	The proposed method only works with elderly patients.
	Method based on multiscale kurtosis and central frequency using wavelet was used [50].	N/A	AO	20 (12 male + 8 female), All healthy	The proposed method only works for healthy patients.
Both machine learning- and envelope-based	Probabilistic-based machine learning method was used for discarding low-quality signals and finding peaks of envelopes [53].	With and Without ECG	AO, AC, IM	65, Healthy young; 15, Healthy old; 48 (32 male + 16 female), Increased Heart Rate; 25 (13 male + 12 female), Unhealthy CVD Patient	The proposed technique did not produce a good result for elderly or unhealthy patients.
Machine learning-based	Three different binary classifiers were used namely naive bayes, logistic regression, and support vector machine [54].	N/A	AS, MC, IM, AO, IC, RE, AC, MO, RF	20 (12 male + 8 female), All healthy	The proposed method relies on ECG to help annotate the SCG peaks.
Visual inspection and	Multichannel SCG and ECG was used [55].	Echo-cardio images	LCV, SCV, AF, PF, MF(A), MF(E)	25 (13 male + 12 female), All healthy	The proposed method only considers the signal acquired from single point on the chest.
Comparison based	Pearson linear correlation coefficient was used for finding the relation [56].	Ultrasound images	AS, PAI, MC, AO, PSI, AC, MO, EVF	42 (20 male + 22 female), All healthy	The proposed method uses very low temporal resolution images. Only 2–4 consecutive cardiac beats were considered at a time.

5. Recent Works

In this section, we present some of the recent works contributed to the SoTA of SCG. In [57], a study focused on temporal changes in the fiducial points of SCG signal was proposed. These changes in signal morphology were dependent on the placement of different sensors on the sternum. In long-term cardiovascular monitoring, SCG offers a variety of alternatives. However, little information is present regarding SCG signal morphology of infants and kids. In [58], it was proposed a highly specialized system which processed both SCG and ECG data of healthy infants and kids between 0–14 years of age. A detailed analysis of different SCG features with regard to amplitudes and time intervals was performed. The infant's SCG amplitude was up to five-times smaller, but the actual signal morphology is the same. In [59], a novel method for SCG template generation was proposed. The method was based on the K-means clustering algorithm and the waveform alignment capability of the dynamic time warping algorithm.

In [60], SCG was used to estimate the cardiorespiratory fitness, and it was calculated by measuring the maximal oxygen consumption (VO₂max) during intense exercise. A non-exercise prediction model for VO₂max was proposed, which used the amplitude and timing interval information extracted from SCG signals. In [61], a novel method for removing the motion artifacts from SCG signals was contributed. The proposed method used adaptive recursive least squares filters for removing the motion artifacts. In [62], the kinetic energies and their temporal integrals in linear as well as rotational dimensions were computed according to both SCG and BCG signals. A study was conducted to test that the kinetic energy from SCG and BCG are related to sympathetic activation during maximal voluntary end-expiratory apnea. The experimental results have shown that maximal end expiratory apnea increases cardiac kinetic energy, which will be useful to assess sympathetic nerve changes in patients with sleep disturbances.

In [63], SCG was used for measuring the pulmonary artery pressure (PAP) by estimating the cardiac timing intervals and hemodynamic parameters such as stroke volume. The results show strong correlation between changes in PAP mean and changes in the SCG-dorso-ventral signal, this means that it has potential to remotely monitor HF patients. In [64], a unified method for assuring the SCG signal quality was proposed. The distance between a signal and reference template was obtained using the dynamic-time feature matching method, which defines signal quality index as a function of the inverse distance between a large set of template signals and the SCG signal. In [65], a neural network-based method was proposed for finding the mapping between SCG and BCG signals; thus, BCG data can be acquired using wearable accelerometers. The newly introduced UNet architecture was used for finding the mapping. In [66], an automated unsupervised procedure was proposed for the analysis of SCG signals through timing annotation. Initially, a suitable heartbeat template was extracted based on SCG traces. Then, timing annotation was performed in two stages: firstly, candidate beats were identified using suitable detection signals, and then, timing annotation was done by aligning candidate beats to the extracted template.

In [67], a noncontact based approach was proposed for acquisition of SCG signal based on the analysis of the reflections of millimeter-wave radar signals. The approach used the hybrid architecture that included a 4D Cardiac Beam former which focused on the reflections of the heart and then a deep learning-based approach was used for transforming these reflections into SCG waveforms. Recently, the coronavirus pandemic (COVID-19) pointed out the need to simplify the process of data collection in intensive care unit particularly for the critically ill-patients [68]. The SCG-based acquisition of cardiac data may be a useful tool to serve the particular need. In [69], an approach for annotation of AO peak was proposed. The SCG signal was acquired using a noncontact method based on microwave Doppler radar. The radar displacement signal of heartbeat (RDH) was used as the reference signal for locating the cardiac cycle and masking the systolic profile to annotate the AO peak. The radar signal was passed through band pass filter followed by application of complex Fourier transformation to get the RDH.

In [70], a delineation framework was introduced to simultaneously identify both systolic and diastolic fiducial points of SCG signals. The proposed method used the wavelet-based scalographic PPG, and an envelope construction scheme to estimate the prominent peaks. Three fiducial points of SCG diastole and three of SCG systolic phase was estimated using a set of amplitude-histogram-based decision rules. To enable the adoption of SCG signal for continuous noninvasive monitoring of hemodynamic parameters in outside-of-hospital settings, a novel denoising pipeline-based method for accurate detection of SCG fiducial points was proposed in [71]. An ensemble empirical mode decomposition method was used to decompose the SCG signal. The corrupted part of the decomposed signal was then removed using the quasiperiodicity behavior of the SCG signal. Finally, the unreliable SCG beats were removed using the quality assessment of the reconstructed SCG beats. The proposed denoising framework can be used to recover usable SCG signal from vehicle-corrupted SCG signals. In [72], SCG signals-based method was proposed for the measurement of the heart rate variability (HRV). The AO peak of SCG signal was estimated using a modified variational mode decomposition-based approach combined with a decision-rule-based scheme. The tachogram of AO–AO intervals was used for the estimation of the HRV parameters. Experimental results showed the effectiveness and strong correlation of the proposed method with standard ECG based analysis.

In [73], both SCG and BCG signals were combined together to produce a novel technique called kinocardiography (KCG) for recording myocardial functions. The body motion produced due to myocardial contractions and flow of blood through cardiac chambers were measured as 12 degrees-of-freedom for combining SCG and BCG signals. The KCG parameters derived from BCG/SCG signals showed high repeatability. In [74], an automatic and remotely controlled system based on multidimensional SCG was used to detect the real-time changes in myocardial contraction during acute myocardial ischemia. It also provides a quantitative assessment of cardiac kinetic energy computed from SCG signals. The experimental results showed that the proposed system empower the healthcare providers and patients to remotely monitor the real-time abnormalities of cardiac health. In [75], SCG and BCG were used for assessing the twist mechanics of left ventricle.

In [76], a novel technique based on contactless wearable patch to remotely record SCG signals is proposed. The technique makes use of stretchable, piezoelectric thin films, and near-field communication technology to power the patch and record the SCG data wirelessly. In [77], the feasibility of using the SCG and gyrocardiac signals for biometric recognition purposes was investigated. A deep learning-based technique using the concept of transfer learning is used for evaluating the existence of discriminative characteristics in SCG and gyrocardiac signals. The results obtained showed that promising recognition rates could be achieved by properly placing the signal acquisition devices.

In [78], clinical status of the heart failure patients were assessed using the application of machine learning algorithms on SCG signal obtained from wearable sensing patches. In [79], machine learning algorithms were used on SCG signal during the cardiopulmonary exercise testing for assessing the status of heart failure patients. In [80], an evolving fuzzy neural network based method was proposed for automatic prediction of the artefactual beats present in the SCG recordings.

6. Experimental Analysis Using SCG

This section presents some of the experimental analysis carried out in the existing literature for assessing the SCG-based cardiac health monitoring procedure. To assess the performance of the proposed methodologies, different matrices were monitored. In this paper, we present the performance of different proposed analysis in terms of precision and sensitivity.

In [30], 5 patients, 3 normal and 2 abnormal, each consisting of 20 cardiac cycles were analyzed for identifying 9 different fiducial points such as, AS, MC, IM, AO, IC, RE, AC, MO, and, RF. The performance results are shown in Figure 8a. The higher outcome of true positive rate, i.e., sensitivity, indicates that the method is efficient in selecting the correct

important points of ECG and SCG signal. In [33], cardiac anomaly detection mechanism based on the investigation of various feature points of SCG signals was proposed. The performance evaluation was carried out on 12,000 cardiac cycles collected from 5 real patients, out of which 3 were normal and 2 were abnormal. For each patient, the evaluation parameters precision and sensitivity were calculated and reported in Figure 8b. The results shows that the SCG annotation mechanism is efficient, as indicated by higher value of precision and sensitivity. The SCG annotation mechanism performed better for the normal subjects compared to that of the abnormal one. The possible reasons behind the reduced performance for the abnormal subjects may be the missing feature points, abnormal morphology, presence of external noise, overlapping of waves, etc. This can be improved marginally by preprocessing the SCG signal by using the data-smoothing techniques.

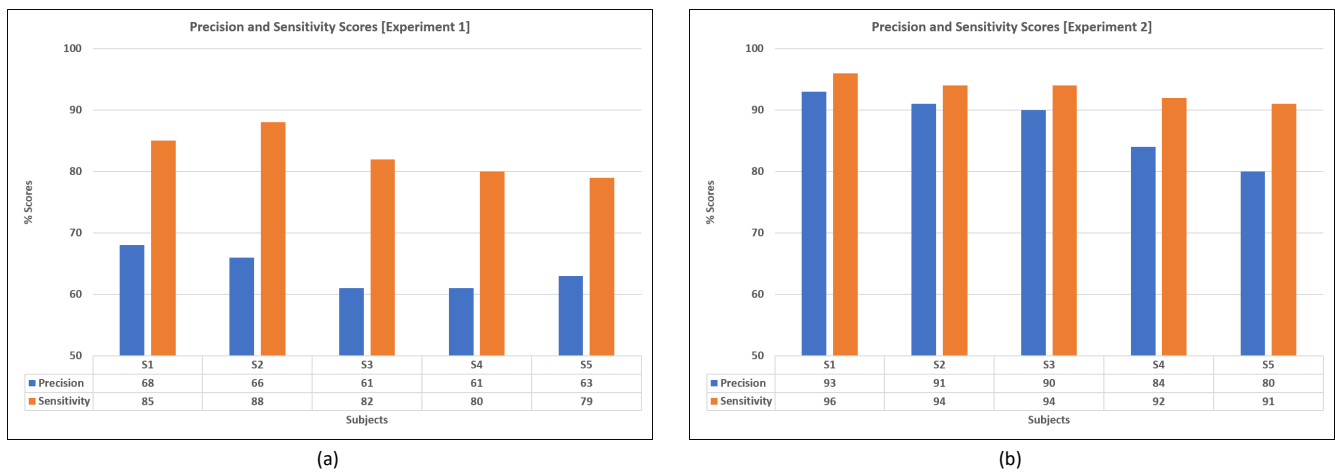


Figure 8. Precision and sensitivity values of (a) Experiment 1, (b) Experiment 2.

In [50], a SCG AO-peak detection framework was proposed. The data from 20 healthy individuals were considered. The performance of the proposed framework is reported in Figure 9a. The results shows that the SCG recordings of subject S1, S3, S11, S14, S18, and S20 produces more false positives which results in low precision value, and the recordings of subject S12, S16, S17, and S18 produces more false negatives, which results in low sensitivity value. Subject S3 and S20 gives maximum false positives across all the records in the database due to their distorted beats and spurious spikes. Thus, by eliminating these two records, the overall performance may increase. In [81], a methodology for annotating MC, IM, AO, AC, and, MO fiducial points of SCG signal was contributed. SCG traces of 15 patients having 3375 cardiac cycles were analyzed and the corresponding performance results are shown in Figure 9b. The results shows that in terms of precision, the proposed method achieves high scores, just 1% of identified peaks are false positives, this may imply that detected premature beats are actual beats. In terms of sensitivity, the result is bit low due to more stringent requirements for a full match, i.e., no data are actually discarded.

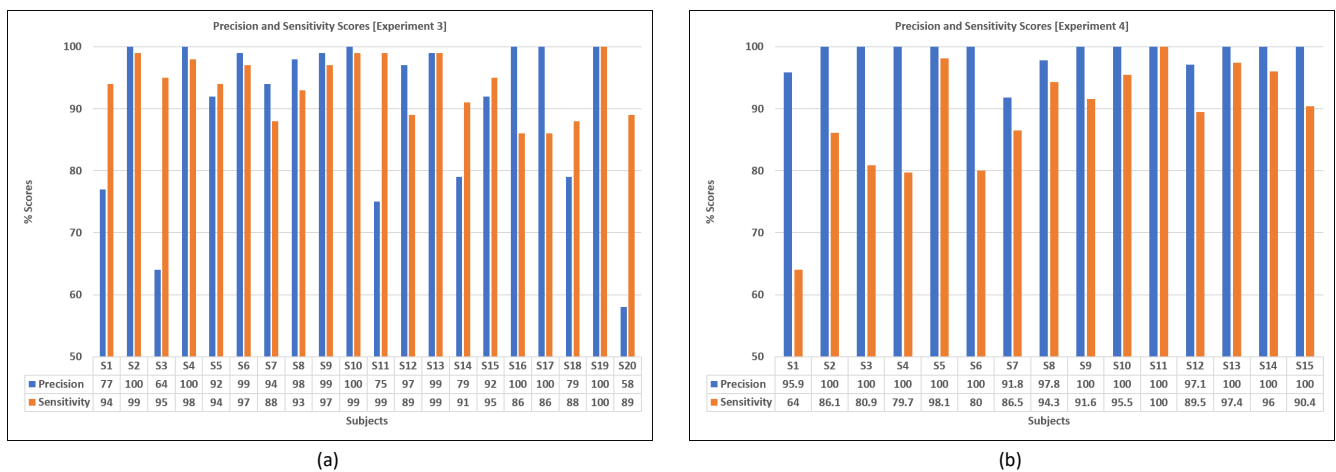


Figure 9. Precision and sensitivity values of (a) Experiment 3, (b) Experiment 4.

Several SCG peak retrieval methods were proposed in [54] for the automatic annotation of SCG signals. The annotation scheme was formulated as a binary classification problem. Three binary classifiers such as NB, SVM, and LR were used for the annotation. The performance evaluation was carried out using 9000 cardiac cycles taken from 20 healthy patients. The outcomes of the proposed classifiers are shown in Figure 10a. Results showed that LR outperformed the other classifiers, and NB consistently performed poorly. The results also showed that with the increase in the number of testing cardiac cycles, the quantitative performance decreases marginally for all annotation schemes. In [82], an AO-peak identification technique was introduced. SCG signal analysis of 25 patients in two different states, rest and postexercise states, were carried out. The performance is shown in Figure 10b. The results shows the better computational efficiency of the proposed algorithm with average 96.6% sensitivity and 99.6% precision for the AO point detection.

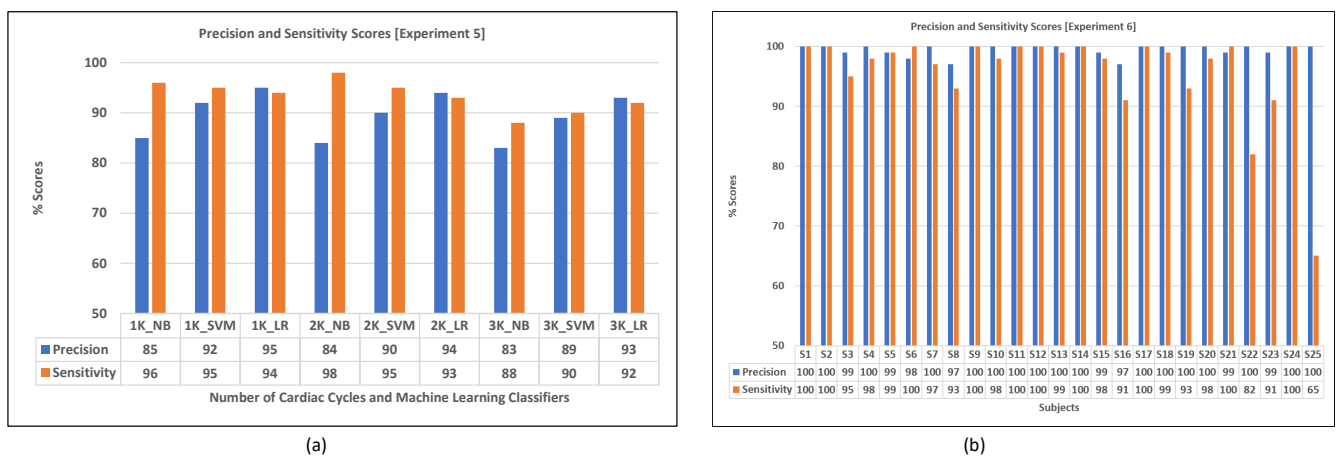


Figure 10. Precision and sensitivity values of (a) Experiment 5, (b) Experiment 6.

Recently, a framework for delineation of SCG signals was proposed in [70]. The method was analyzed on eight male patients in two different breathing patterns: i.e., normal and stopped breathing. The performance of the proposed delineation framework was analyzed corresponding to IM, AO, IC, AC, and MO points. The results are shown in Figure 11. The results show that the proposed method achieves the average precision and sensitivity score of 97.8% and 97.16%, respectively, on the normal breathing database, while 95.33% and 93.5%, respectively, on the stopped breathing database. This higher sensitivity and precision score indicates better performance for the detection of AO peak.

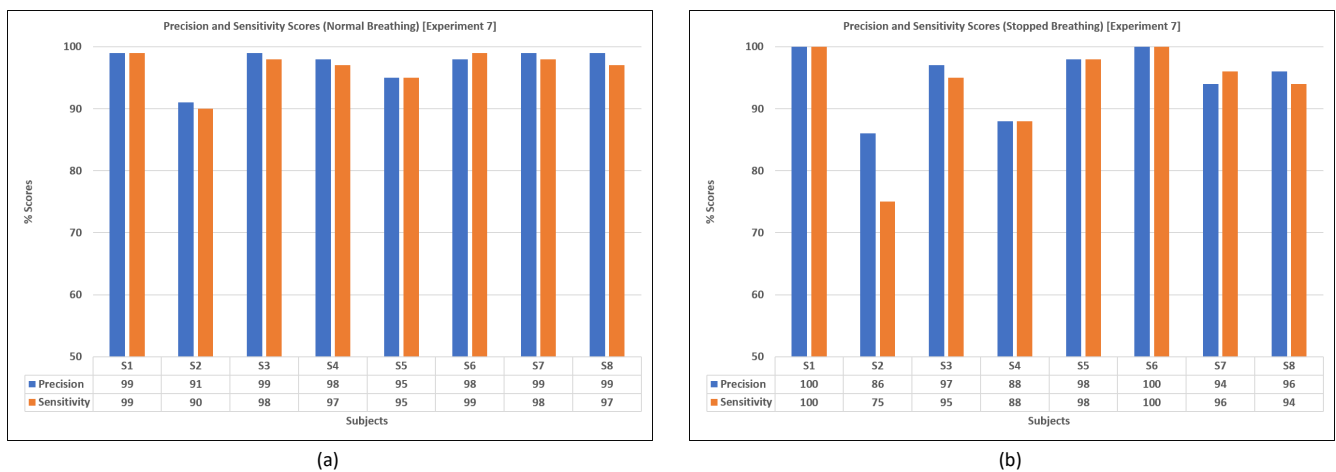


Figure 11. Precision and sensitivity values of (a) Experiment 7 (normal breathing state), (b) Experiment 7 (stopped breathing state).

In [83], an AO-peak annotation technique based on machine learning binary classifiers was proposed. A total of six patients accounting for 1800 cardiac cycles were analyzed. The results corresponding to each classifier are shown in Figure 12a. The results shows that GNB outperforms the other classifiers for AO-peak detection. In [84], a binary classifier-based methodology was described for the annotation of IM and AC points of SCG signals. A total of three patients accounting for 948 cardiac cycles were analyzed. The reported results corresponding to each classifier are shown in Figure 12b. The results show that the overall performance of RF is better in comparison to that of other classifiers.

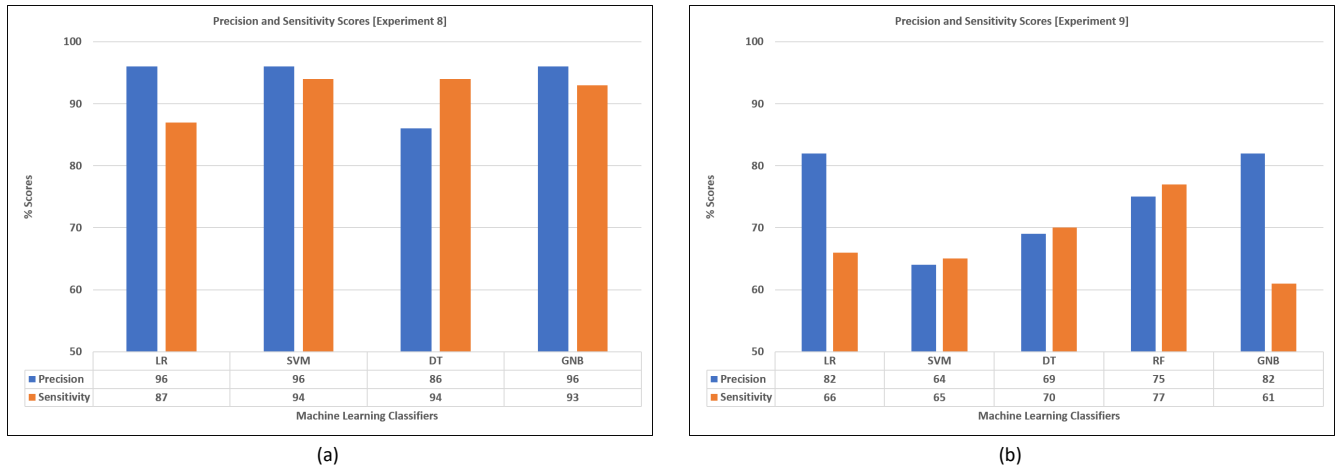


Figure 12. Precision and sensitivity values of (a) Experiment 8, (b) Experiment 9.

The overall details corresponding to the number of patients considered (#Sub), number of cardiac cycles (#CC) and data points analyzed (#DP), identified feature points (FP), and mean precision (Mean_Prec) and mean sensitivity (Mean_Sens) values of the above discussed experimental analysis are shown in Table 4. The comparative analysis of all the experiments in terms of mean precision and mean sensitivity values are also shown in Figure 13. Experiment E6 delivered better results for feature point detection. This is because in this experiment, the SCG signal was together with the GCG signal for recording purpose, which records the angular cardiac vibrations in addition to normal vibrations, which helps in achieving better results. Furthermore, the overall performance of experiments E3, E6, and E8 are better in comparison to that of other experiments. This shows that it is easier to detect or identify the AO peak of the SCG signal, which is the most prominent peak.

Table 4. Details of conducted experiments.

Experiment	#Sub	#CC and #DP	FP	Mean_Prec	Mean_Sens
Experiment 1 [30]	5	CC: 100, DP: 35609	AS, MC, IM, AO, IC, RE, AC, MO, RF	63.8	82.8
Experiment 2 [33]	5	CC: 3243, DP: 30102	AS, MC, IM, AO, IC, RE, AC, MO, RF	87.6	93.4
Experiment 3 [50]	20	CC: 20, DP: 4585	AO	90.1	93.8
Experiment 4 [81]	15	CC: 3375, DP: –	MC, IM, AO, AC, MO	88.7	98.8
Experiment 5 [54]	20	CC: 9000, DP: –	AS, MC, IM, AO, IC, RE, AC, MO, RF	89.4	93.4
Experiment 6 [82]	25	CC: 50, DP: 23984	AO	99.4	95.8
Experiment 7 [70]	8	CC: 16, DP: 6854	IM, AO, IC, AC, MO	96.0	94.9
Experiment 8 [83]	6	CC: 1800, DP: 3985	AO	93.5	92.0
Experiment 9 [84]	3	CC: 948, DP: 5678	IM, AC	74.4	67.8

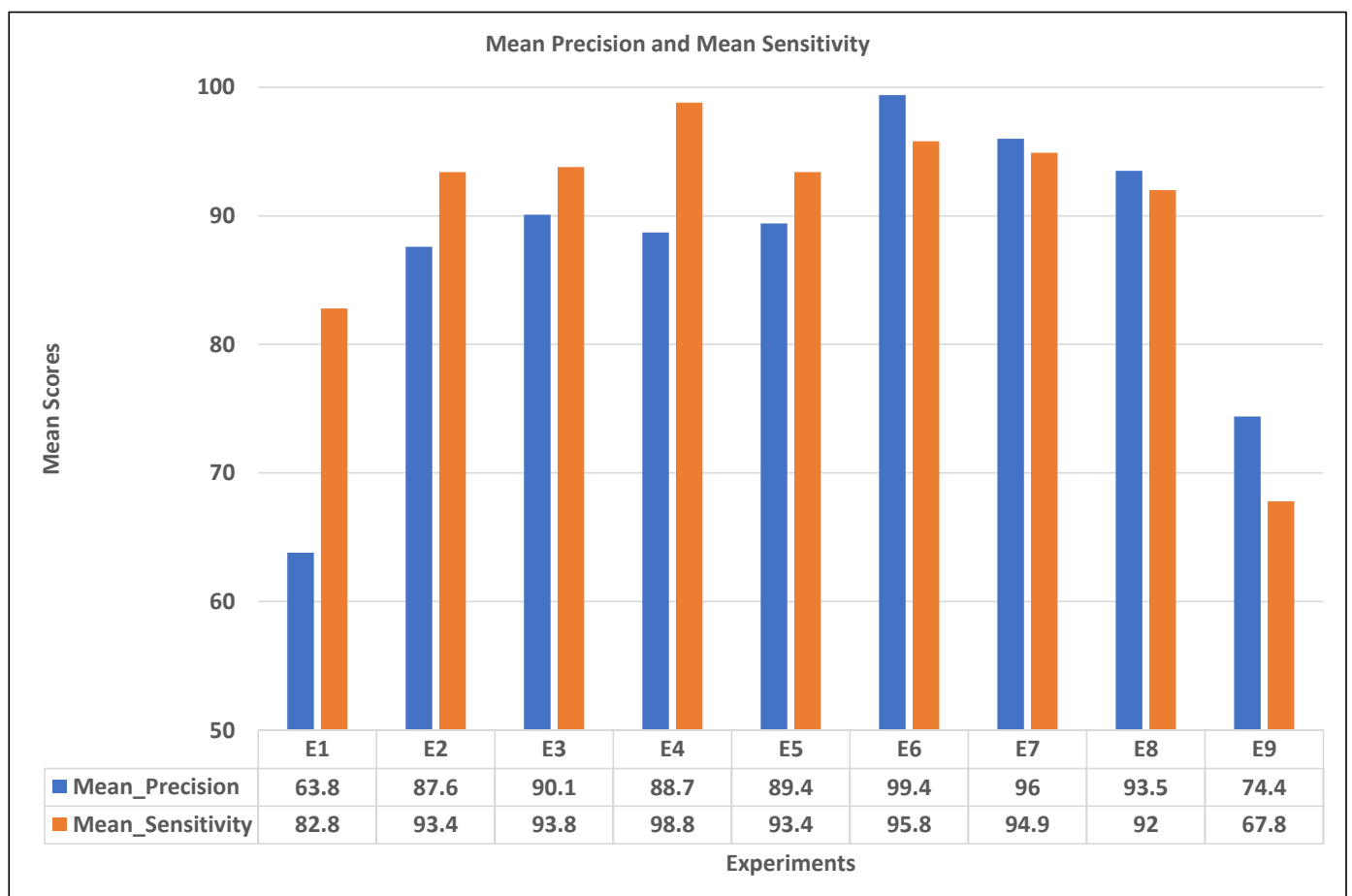


Figure 13. Mean precision and mean sensitivity values of all experiments.

7. Applications

Seismocardiography provides the potential for regular monitoring of cardiac activities, both in the clinic and home [85]. SCG facilitates the measurement of time devoted by heart during different cardiac activities and phases that provide significant insight into different cardiovascular functioning. These times are primarily known as CTI. SCG finds its application in monitoring cardiac health and the detection of different cardiac diseases using the extracted timing information.

7.1. Extraction of CTI for Cardiac Health Monitoring

CTIs are defined for both the systolic and diastolic phases of the cardiac cycle. The extraction of different cardiac timing intervals based on these phases is discussed in subsequent sections. The overall comparison of the different extracted intervals is presented in Table 5.

Table 5. Comparison of extracted CTIs.

Cardiac Phase	Parameter Extracted	Physiological Event	Interval/Ratio	Methodologies Used for Extraction
Systolic	S_1S_2	First and second heart sound	MC – AC	(i) Comparison and combined analysis of different cardiac parameters and signals such as ECG, PCG, ICG, etc. [86–91]. (ii) Regression model [92–94]. (iii) Tissue doppler imaging method [95].
	QS_2	Total systole interval	Q – AC	
	Q–I	Interval from onset of QRS to S_1	Q – MC	
	PEP	Pre-ejection period	Q – AO	
	LVET	Left ventricular ejection time	AO – AC	
	IVCT	Isovolumetric contraction time	MC – AO	
	PEP/LVET	Contractility coefficient	$(Q - AO)/(AO - AC)$	
Diastolic	LVFT	Left-ventricular filling time	MO – MC	
	RVFT	Rapid ventricular filling time	MO – RF	
	IVRT	Isovolumetric relaxation time	AC – MO	
Global	MPI	Myocardial performance index	$(IVCT + IVRT)/LVET$	

7.1.1. Extraction of Systolic Time Interval

The term systole time interval (STI) was first used almost 145 years ago. In [96], it was discussed that the interval length between commencement of the ventricular systole and the closure of the AV does not change when the pulse-rate is constant. In a study published in [97], the diastolic part of the cardiac cycle was shown to shorten faster than systolic with increasing pulse-rate, but the systole is always shorter than diastole. Later in [98], it was contradicted and shown that the diastole is shorter than systole when the pulse rate exceeds 135 per minute.

In [86], the potential usefulness of STI was studied by measuring the systole interval of LV using simultaneous recording of the ECG, PCG, and the carotid arterial pulse tracing. The intervals identified were QS_2 , LVET, S_1S_2 , PEP, IVCT, and Q-I as shown in Table 5. In [87], an algorithm based on heart sound and ECG was proposed for automatically extracting PEP and LVET. Heart sound was used to accurately measure the opening and closing moments of the AV valve. The Bayesian approach was used for estimating PEP and, since AV closure corresponds to the second heart sound, its onset was used for estimating LVET. In [88], a novel method was proposed for measuring PEP and LVET based on the combined analysis of ECG, ICG, and SCG in head-to-foot direction, in place of dorso-ventral direction. Additionally, the effect of postural variations was examined on the correlation of estimated values of PEP and LVET from SCG and ICG.

In [89], a comparative study regarding the investigation of the accuracies of extracting CTIs based on PCG, ICG, and SCG w.r.t. multimodal echocardiography technique was contributed. ECHO used doppler, tissue doppler imaging, and m-mode methods as clinical standards. The study showed that, in comparison to ECHO, the accuracies of the estimation of PEP were 43%, 43%, and 86% for PCG, ICG, and SCG, respectively. Corresponding to the estimation of QS_2 it was 80%, 43%, and 90% for PCG, ICG, and SCG respectively. In summary, SCG outperformed the other compared techniques.

In [92], a regression model was adopted for accurately estimating the SCG based PEP. Initially, the set of timing features was extracted by placing SCG sensors at different locations, and later a regression model was proposed for combining all the extracted features. The model was trained on the extracted features from ensemble averages and their corresponding PEP. Next, the trained model is used to estimate the PEP value. In [93], another regression model was introduced for estimating PEP. The individual data of accelerometer-based SCG and gyroscope based SCG was combined and a regression

model was trained. The trained model was then used for the estimation of PEP. Gyroscopes, in combination with accelerometers, were found to provide a better estimation of PEP.

7.1.2. Extraction of Diastolic Time Information

In [90], CTIs were calculated for patients suffering from myocardial infarction with ischemia. The calculation was carried out during an exercise tolerance test concerning ECG. Different systolic, diastolic, and global parameters were identified and accordingly presented in Table 5. In [91], an SCG-based methodology was proposed for predicting the diastolic time vibration. AC and MC points of SCG were selected as they do not change significantly from one cardiac cycle to another. The ECG Q-wave was used as a reference. The average of QAC interval was used for predicting the start of diastole and the average of Q-MC interval was used to predict the end of diastole. In [95], the tissue doppler imaging method was used for determining diastolic time features for the assessment of LV function. CTI was calculated based on a comparison of the onset time of the early diastolic velocity of the mitral annulus and the onset time of mitral inflow.

7.2. Atrial Fibrillation

In [99], an in-home application-based monitoring tool was contributed for automatically detecting the Atrial fibrillation (AFib) using BCG signals. The same tool can be used with SCG signals. Machine learning-based classification algorithms were used. Seven different algorithms were evaluated and ranked using a 10-fold cross-validation method. Random forest achieved the best result with mean specificity and mean sensitivity of 0.982 and 0.938, respectively. In [100], an SCG-based technique was proposed for detecting the AFib. Linear least-squares classifier was proposed with logarithmic heart rate variability index and spectral entropy as the input. The leave-one-out cross-validation method was used which achieved 99.9 % and 96.4 % average true positive rate and average true negative rate, respectively, for detecting AFib.

In [101], an in-built accelerometer and gyroscope of a smartphone were used for detecting the AFib. Three different machine learning classifiers were used: support vector machine (SVM), kernel SVM, and random forest. The leave-one-person-out cross-validation method was used for evaluation. Kernel SVM classifier achieved the best result with 100% specificity and 93.8% sensitivity in the case of majority voting. Without majority voting, the specificity was 98.7% and sensitivity was 84.7%. The same approach was comprehensively analyzed in [102] with more features. Additionally, the latter approach was evaluated using both cross-validation (CV) and cross-database (CD) data. Results showed specificity and sensitivity of approximately 95% and 99%, respectively, for the CV data, and 97% and 93% for the CD data, respectively. In [103], population based approach for modeling AFib was presented. In [104], pulmonary vein activity was studied to determine the AFib recurrence.

7.3. Cardiac Computing Tomography Gating Based on Quiescence Prediction

In [105], SCG was used in addition to ECG for strengthening the cardiac computed tomography angiography (CTA) process. It is crucial to accurately predict the quiescent phases for gating CTA. SCG was found to be a good predictor of quiescence, but whenever there is an increase in the heart rate, ECG-based prediction performs well. Thus, it was concluded that by combining SCG and ECG the performance of real-time gating for cardiac CTA can be improved significantly. In [106], a three-layer artificial neural network (ANN) model was proposed for combining the ECG and SCG based quiescence predictions for gating CTA. The combined ECG-SCG ANN model achieved 47% more cardiac quiescence prediction on average in comparison to that of ECG-alone. In [107], SCG was used with electrocardiogram for detecting the cardiac quiescent phases, which were used for gating CTA. Thus, the relationship between electrical and mechanical activities of the heart was characterized. AV closure and its corresponding time position on electrocardiogram were used for visualizing the cardiac quiescent phases with respect to heart rate.

In [108], two different methods were presented for addressing the problem of cardiac quiescent period detection. First, the real-time quiescence period was detected using beat-by-beat analysis of SCG. This approach was affected by both the sensor noise and the movement of the patient. Second, the other method used the velocity magnitude of the chest wall movement extracted from SCG signals using Kalman filter. For healthy patients, the average systolic and diastolic quiescent periods were centered at 29% and 76%, respectively; for unhealthy patients, it was 33% and 79%, respectively. In [94], low-velocity components of cardiac cycles were identified for segmenting different cardiac quiescent phases. The study was based on the synchronous assessment of both SCG and ECG.

7.4. Heart Rate and Heart Rate Variability Index

In [109], a method based on Hilbert transform was proposed for monitoring the heart rate (HR) using SCG signals. Heartbeat timings and inter-beat time intervals were measured from SCG signals in supine, left, and right recumbent positions. In [110], a hidden Markov model-based approach was described for processing the SCG signals and the expectation-maximization algorithm was used to learn its morphology. The processed signal was used for obtaining the Viterbi sequence using the Viterbi algorithm. The Viterbi sequence was finally used for estimating HR. In [111], an approach for estimating the HR during high- and low-lung volume phases was proposed. The lung volume information was extracted using the respiratory flow rate from SCG signals. The extracted low- and high-lung volume SCG events were used for estimating the HR. Patients with high-lung volume had higher HR.

In [112], the combination of both the six-axis accelerometer and the gyroscope SCG signals were used for estimating the HR. The signals were standardized and combined using ensemble averaging. Finally, only the dominant frequencies were used for HR estimation. In [113], HRV indices obtained from SCG and ECG signals were compared and the influence of the heartbeat detector on SCG signals was determined. The signals were obtained from the combined measurement of ECG, breathing, and SCG (CEBS) database. Another comparison of HRV indices obtained from ECG, SCG, PCG, photo-plethysmography, and piezo-plethysmography was done in [114]. In [82], a real-time HR monitoring system was proposed based on combined SCG and GCG. The windowed approach was used and the waveforms were analyzed in three different phases within each window. Finally, the weighted mean was used to combine the results of all the windows and one final HR per time step was calculated.

Recently, in [66] a completely unsupervised automated process for HR monitoring based on SCG signals was introduced. The process was divided into two subtasks: first, candidate beats were identified and validated, and next, timing annotation was done. In [115], a Convolutional Variational AutoEncoder based unsupervised method was proposed for extracting the heartbeat complexes and the associated morphological informations. In [116], a SCG-based approach was proposed using wavelet decomposition, Fourier-based envelope detection, and time-averaged power spectral density for the estimation of HR. Finally, a SCG-based approach was contributed in [117] for the analysis of HRV. The heartbeats in SCG were detected as the peak within 100ms window from the occurrence of ECG-R wave.

7.5. Myocardial Ischemia

In [21], LV function was monitored through SCG analysis for myocardial ischemia diagnosis. In [118], changes in cardiac muscle contractility due to exercise was studied using SCG analysis. The findings were used for the diagnosis of ischemia in patients with coronary artery disease. Further, the results were compared with the electrocardiographic exercise test, and using the SCG-based diagnosis was found to be more sensitive and accurate. In [119], a Fast Fourier Transformation-based real-time analysis of SCG was carried out on pigs. Discrimination was found between different intra- and postoperative causes of myocardial ischemia. In [21], changes in LV function of a patient suffering from ischemia were monitored. The amplitude of MC, RE, RF, and AS points of SCG was

measured, and three different ratios with respect to RE point were calculated. The AS/RE, MC/RE, and RF/RE ratios considerably helped in monitoring the LV function during myocardial ischemia. Lastly, three different CTIs, PEP, LVET, and QS2 were used in [120] for determining the LV performance during ischemia.

7.6. Myocardial Contractility

In [121], myocardial contractility was monitored during hyperbaric exposure using SCG. The approach was able to record, amplify, and transfer the signal to an outside system with an acceptable signal-to-noise ratio. SCG was found to be an easy-to-use, noninvasive method for surveillance of myocardial contractility. In [122], two features, i.e., LV pressure and stroke volume, were extracted from SCG for monitoring myocardial contractility. The correlation of these two features with SCG was found based on the study carried over three pigs. The study presented a patient-specific solution for estimating the stroke volume, which was used for monitoring the myocardial contractility.

7.7. Pulse Transit Time (PTT)

In [123], the AO point on SCG was used for measuring the PTT and finding its correlation with pulse pressure. In [124], the acoustic sensor was used together with SCG for measuring the PTT. Firstly, AO peaks were located on SCG and the corresponding acoustic peak was located within the 200 ms window after the AO peak. Next, PTT was calculated by taking the difference between AO and acoustic peak. The same approach was further enhanced in [41] by taking into account the comparison of SCG and photoplethysmogram recordings. The results obtained could be useful for the development of a BP monitoring system.

7.8. Respiratory Information

In [125], an algorithm was proposed to extract the respiratory information from SCG signals. Three features were extracted, namely, intensity modulation, timing interval changes (within each heartbeat), and timing interval changes (between successive heartbeats). A respiration belt was also used to measure the respiratory information, and it was close to SCG-based information. In [126], cardiac vibrations were used to find cardiopulmonary health. Respiration effect was investigated on the frequency domain of the SCG signal. The frequency domain of the SCG analysis outperformed the time-domain analysis. In [127], a machine learning-based algorithm was developed to analyze SCG signals for identifying the respiratory phases. The SVM model was used instead, and it successfully identified 88% of the phases.

7.9. Fetal Surveillance

In [128], gyrocardiogram and SCG recordings were collected from abdominal inertial sensors for detecting the fetal HR. In [129], a novel application of fetal surveillance was proposed based on noninvasive fetal ECG (NIFECEG) technique, which can further be extended for SCG.

7.10. Cardiac Stress Monitoring

In [130], an ultra-short HRV index was used to detect the changes during cardiac stress. In [131], SCG was used as an alternative to ECG for cardiac stress monitoring during MRI.

7.11. Cardiac Hemorrhage

A portable and cost-effective solution for detecting the mild cardiac hemorrhage based on the measurement of PEP and LVET was proposed in [132].

7.12. Other Applications

In [133], an SCG-based approach was introduced to identify the abnormality in the aortic flow. In [134], a Deep Convolutional Neural Network (D-CNN)-based approach

was proposed for robustly monitoring the cardiac activity from SCG signals. In [135], SCG was considered for monitoring the left ventricular function of the cancer patients using the assessment of cardiotoxicity. In [136], mathematical model for human heart left-ventricle was presented. In [137], role of ionic modeling on cardiac arrhythmias was presented for both healthy and diseased heart.

8. Summary and Open Issues for Future Research

The recent advancements in the SCG field have strong potential to address the cardiac health of individuals, especially outside the clinic. This review showed that the SCG technique was extensively applied for the diagnosis of different cardiac anomalies. Nevertheless, several open issues need to be addressed in the field of SCG, which can improve understanding of the technique and its clinical applicability in the near future. Some of these key challenges are in regards to the field of computer-aided healthcare diagnosis [138]. Additionally, we identified the following issues and future scope in the existing studies:

- Few studies focused on using a robust documentation of the relationship between feature points and their physiological sources. It would be useful to investigate the relationship between SCG waves and cardiac activities.
- SCG variability is affected by several factors including respiratory phases, gender, age, sensor location, health conditions, cardiac contractility, heart rhythm, and postural positions. A deeper study of these factors will enhance understanding of SCG signals and can guide to achieve better groupings of similar SCG events to reduce variability and noise. It may also lead to a more accurate definition of SCG features points.
- Existing data acquisition is mostly based on contact sensors attached to the skin, which is irritable and produces skin coupling. Therefore, efficient contactless SCG detection techniques would be needed.
- Continuous monitoring might help in the early detection of serious cardiac conditions and potentially reduce cardiac health care costs. Currently, very few systems are available for at-home and continuous monitoring. An efficient at-home data acquisition system could be developed for regular monitoring.
- Assessment of day-to-day cardiac mechanical variability may help in the development of a robust SCG analysis system.
- Studies show that the SCG signal is mostly contaminated by motion-artifacts. Techniques for removing noises in ambulatory settings need to be developed.
- Several machine learning approaches were applied for determining feature points. Nevertheless, it may be applied for other different purposes in SCG studies, including classification into different phases of the respiratory cycle, calculation of cardiac time intervals, and classification of patients into high-, low-, and normal-risk.
- Fetal surveillance is a new area where SCG can be applied for monitoring HR and respiratory phases.
- SCG can be applied for monitoring the cardiac health of patients with epilepsy.

In summary, robust signal processing techniques and physiological understanding of the SCG signal could assist with the development of a powerful at-home monitoring tool and promote clinical applicability for cardiac health.

9. Conclusions

In the existing literature, few studies focused on the relationship between feature points and their physiological sources. In this comprehensive review, Table 2 summarized all the feature points in the field together with their corresponding physiological events and referential identifiers. Moreover, the acquisition techniques were not summarized or categorized until now. Table 1 summarized different acquisition techniques proposed in the SoTA. Additionally, the annotation techniques present in the SoTA were not summarized or categorized either; Table 3 summarized different annotation techniques by proper categorization to improve understanding. Finally, few studies were focused on performing a detailed study of the areas of application of SCG; Section 7 introduced a detailed discussion

about various areas of application to be addressed in the future. This work ends with the proposal of several alternatives for tackling many of the open issues introduced here.

Author Contributions: Conceptualization, H.K.T. and D.R.; methodology, H.K.T., J.S. and D.R.; software, D.R. and S.S.R.; validation, D.R., C.B. and J.S.; formal analysis, F.R., C.B. and S.S.R.; investigation, H.K.T. and J.S.; resources, D.R.; data curation, F.R., C.B. and S.S.R.; writing—original draft preparation, D.R. and H.K.T.; writing—review and editing, F.R., H.K.T., J.S., S.S.R.; visualization, F.R. and D.R.; supervision, H.K.T. and J.S.; project administration, H.K.T. All authors have read and agreed to the published version of the manuscript.

Funding: This research received no external funding.

Institutional Review Board Statement: Not applicable.

Informed Consent Statement: Not applicable.

Data Availability Statement: Not applicable.

Conflicts of Interest: The authors declare no conflict of interest.

References

1. Quaglini, S.; Stefanelli, M.; Boiocchi, L.; Campari, F.; Cavallini, A.; Micieli, G. Cardiovascular risk calculators: Understanding differences and realising economic implications. *Int. J. Med. Inform.* **2005**, *74*, 191–199. [[CrossRef](#)]
2. Benjamin, E.J.; Muntner, P.; Bittencourt, M.S. Heart disease and stroke statistics-2019 update: A report from the American Heart Association. *Circulation* **2019**, *139*, e56–e528. [[CrossRef](#)] [[PubMed](#)]
3. Neubeck, L.; Coorey, G.; Peiris, D.; Mulley, J.; Heeley, E.; Hersch, F.; Redfern, J. Development of an integrated e-health tool for people with, or at high risk of, cardiovascular disease: The Consumer Navigation of Electronic Cardiovascular Tools (CONNECT) web application. *Int. J. Med. Inform.* **2016**, *96*, 24–37. [[CrossRef](#)] [[PubMed](#)]
4. Blecker, S.; Austrian, J.S.; Horwitz, L.I.; Kuperman, G.; Shelley, D.; Ferraiuola, M.; Katz, S.D. Interrupting providers with clinical decision support to improve care for heart failure. *Int. J. Med. Inform.* **2019**, *131*, 103956. [[CrossRef](#)]
5. Tison, G.H.; Chamberlain, A.M.; Pletcher, M.J.; Dunlay, S.M.; Weston, S.A.; Killian, J.M.; Olgin, J.E.; Roger, V.L. Identifying heart failure using EMR-based algorithms. *Int. J. Med. Inform.* **2018**, *120*, 1–7. [[CrossRef](#)] [[PubMed](#)]
6. Yanicelli, L.M.; Vegetti, M.; Goy, C.B.; Martínez, E.C.; Herrera, M.C. SiTe iC: A telemonitoring system for heart failure patients. *Int. J. Med. Inform.* **2020**, *141*, 104204. [[CrossRef](#)]
7. Lukkarinen, S. Phonocardiography: Development of a Clinical System and Its Application to Screening for Paediatric Heart Murmurs. Ph.D. Thesis, Aalto University, Espoo, Finland, 2012.
8. Einthoven, W. The string galvanometer and the human electrocardiogram. *Know Proc.* **1903**, *6*, 107–115.
9. Jekova, I.; Vassilev, P.; Stoyanov, T.; Pencheva, T. InterCriteria Analysis: Application for ECG Data Analysis. *Mathematics* **2021**, *9*, 854. [[CrossRef](#)]
10. Starr, I.; Rawson, A.; Schroeder, H.; Joseph, N. Studies on the estimation of cardiac output in man, and of abnormalities in cardiac function, from the heart's recoil and the blood's impacts; the ballistocardiogram. *Am. J. Physiol.-Leg. Content* **1939**, *127*, 1–28. [[CrossRef](#)]
11. Bour, J.; Kellett, J. Impedance cardiography—A rapid and cost-effective screening tool for cardiac disease. *Eur. J. Intern. Med.* **2008**, *19*, 399–405. [[CrossRef](#)]
12. Edler, I.; Lindström, K. The history of echocardiography. *Ultrasound Med. Biol.* **2004**, *30*, 1565–1644. [[CrossRef](#)]
13. Mounsey, P. Praecordial ballistocardiography. *Br. Heart J.* **1957**, *19*, 259. [[CrossRef](#)]
14. Dilsizian, V.; Taillefer, R. Journey in Evolution of Nuclear Cardiology: Will There Be Another Quantum Leap With the F-18-Labeled Myocardial Perfusion Tracers? *JACC Cardiovasc. Imaging* **2012**, *5*, 1269–1284. [[CrossRef](#)]
15. Pauwels, E.; Van Loo, D.; Cornillie, P.; Brabant, L.; Van Hoorebeke, L. An exploratory study of contrast agents for soft tissue visualization by means of high resolution X-ray computed tomography imaging. *J. Microsc.* **2013**, *250*, 21–31. [[CrossRef](#)]
16. White, J.A.; Patel, M.R. The role of cardiovascular MRI in heart failure and the cardiomyopathies. *Magn. Reson. Imaging Clin. N. Am.* **2007**, *15*, 541–564. [[CrossRef](#)] [[PubMed](#)]
17. Tadi, M.J.; Lehtonen, E.; Pankkäälä, M.; Saraste, A.; Vasankari, T.; Teräs, M.; Koivisto, T. Gyrocardiography: A new non-invasive approach in the study of mechanical motions of the heart. Concept, method and initial observations. In Proceedings of the 2016 38th Annual International Conference of the IEEE Engineering in Medicine and Biology Society (EMBC), Orlando, FL, USA, 16–20 August 2016; pp. 2034–2037.
18. Meriheinä, U.; Juppo, M.; Koivisto, T.; Pänkäälä, M.; Sairanen, K.; Grönholm, M. Heart Monitoring System. U.S. Patent 10,178,964, 1 January 2019.
19. Salerno, D.M. Seismocardiography: A new technique for recording cardiac vibrations. concept, method, and initial observations. *J. Cardiovasc. Technol.* **1990**, *9*, 111–118.

20. Agress, C.M.; Fields, L.G. New method for analyzing heart vibrations: I. Low frequency vibrations. *Am. J. Cardiol.* **1959**, *4*, 184–190. [[CrossRef](#)]
21. Salerno, D.M.; Zanetti, J. Seismocardiography for monitoring changes in left ventricular function during ischemia. *Chest* **1991**, *100*, 991–993. [[CrossRef](#)]
22. Crow, R.S.; Hannan, P.; Jacobs, D.; Hedquist, L.; Salerno, D.M. Relationship between seismocardiogram and echocardiogram for events in the cardiac cycle. *Am. J. Noninvasive Cardiol.* **1994**, *8*, 39–46. [[CrossRef](#)]
23. Akhbardeh, A.; Tavakolian, K.; Gurev, V.; Lee, T.; New, W.; Kaminska, B.; Trayanova, N. Comparative analysis of three different modalities for characterization of the seismocardiogram. In Proceedings of the 2009 Annual International Conference of the IEEE Engineering in Medicine and Biology Society, Minneapolis, MN, USA, 3–6 September 2009; pp. 2899–2903. [[CrossRef](#)]
24. Ngai, B.; Tavakolian, K.; Akhbardeh, A.; Blaber, A.P.; Kaminska, B.; Noordergraaf, A. Comparative analysis of seismocardiogram waves with the ultra-low frequency ballistocardiogram. In Proceedings of the 2009 Annual International Conference of the IEEE Engineering in Medicine and Biology Society, Minneapolis, MN, USA, 3–6 September 2009; pp. 2851–2854.
25. Inan, O.T.; Migeotte, P.F.; Park, K.S.; Etemadi, M.; Tavakolian, K.; Casanella, R.; Zanetti, J.; Tank, J.; Funtova, I.; Prisk, G.K.; et al. Ballistocardiography and seismocardiography: A review of recent advances. *IEEE J. Biomed. Health Inform.* **2014**, *19*, 1414–1427. [[CrossRef](#)] [[PubMed](#)]
26. Taebi, A.; Solar, B.E.; Bomar, A.J.; Sandler, R.H.; Mansy, H.A. Recent advances in seismocardiography. *Vibration* **2019**, *2*, 64–86. [[CrossRef](#)] [[PubMed](#)]
27. Feigen, L.P. Physical characteristics of sound and hearing. *Am. J. Cardiol.* **1971**, *28*, 130–133. [[CrossRef](#)]
28. Yang, C.; Tavassolian, N. Combined seismo and gyro cardiography: A more comprehensive evaluation of heart-induced chest vibrations. *IEEE J. Biomed. Health Inform.* **2017**, *22*, 1466–1475. [[CrossRef](#)] [[PubMed](#)]
29. Leitão, F.; Moreira, E.; Alves, F.; Lourenço, M.; Azevedo, O.; Gaspar, J.; Rocha, L. High-Resolution Seismocardiogram Acquisition and Analysis System. *Sensors* **2018**, *18*, 3441. [[CrossRef](#)]
30. Sahoo, P.; Thakkar, H.; Lee, M.Y. A cardiac early warning system with multichannel SCG and ECG monitoring for mobile health. *Sensors* **2017**, *17*, 711. [[CrossRef](#)] [[PubMed](#)]
31. Ha, T.; Tran, J.; Liu, S.; Jang, H.; Jeong, H.; Mitbender, R.; Huh, H.; Qiu, Y.; Duong, J.; Wang, R.L.; et al. A Chest-Laminated Ultrathin and Stretchable E-Tattoo for the Measurement of Electrocardiogram, Seismocardiogram, and Cardiac Time Intervals. *Adv. Sci.* **2019**, *6*, 1900290. [[CrossRef](#)]
32. Mitra, U.; Emken, B.A.; Lee, S.; Li, M.; Rozgic, V.; Thatte, G.; Vathsangam, H.; Zois, D.S.; Annavaram, M.; Narayanan, S.; et al. KNOWME: A case study in wireless body area sensor network design. *IEEE Commun. Mag.* **2012**, *50*, 116–125. [[CrossRef](#)]
33. Sahoo, P.; Thakkar, H.; Lin, W.Y.; Chang, P.C.; Lee, M.Y. On the design of an efficient cardiac health monitoring system through combined analysis of ecg and scg signals. *Sensors* **2018**, *18*, 379. [[CrossRef](#)]
34. Javaid, A.Q.; Ashouri, H.; Dorier, A.; Etemadi, M.; Heller, J.A.; Roy, S.; Inan, O.T. Quantifying and reducing motion artifacts in wearable seismocardiogram measurements during walking to assess left ventricular health. *IEEE Trans. Biomed. Eng.* **2016**, *64*, 1277–1286. [[CrossRef](#)]
35. Etemadi, M.; Inan, O.T.; Heller, J.A.; Hersek, S.; Klein, L.; Roy, S. A Wearable Patch to Enable Long-Term Monitoring of Environmental, Activity and Hemodynamics Variables. *IEEE Trans. Biomed. Circuits Syst.* **2016**, *10*, 280–288. [[CrossRef](#)]
36. Morbiducci, U.; Scalise, L.; De Melis, M.; Grigioni, M. Optical vibrocardiography: A novel tool for the optical monitoring of cardiac activity. *Ann. Biomed. Eng.* **2007**, *35*, 45–58. [[CrossRef](#)] [[PubMed](#)]
37. Xia, Z.; Shandhi, M.M.H.; Inan, O.T.; Zhang, Y. Interference and Removal of Respiration Harmonics on Noncontact Seismocardiogram Signals. *Struct. Health Monit.* **2017**, *2017*. [[CrossRef](#)]
38. Xia, Z.; Shandhi, M.M.H.; Inan, O.T.; Zhang, Y. Non-Contact Sensing of Seismocardiogram Signals Using Microwave Doppler Radar. *IEEE Sens. J.* **2018**, *18*, 5956–5964. [[CrossRef](#)]
39. Shirkovskiy, P.; Laurin, A.; Chapelle, D.; Fink, M.; Ing, R. Contactless mapping of thoracic and abdominal motion: Applications for seismocardiography. In Proceedings of the 2017 Computing in Cardiology (CinC), Rennes, France, 24–27 September 2017; pp. 1–4.
40. Yang, C.; Tang, S.; Tavassolian, N. Utilizing gyroscopes towards the automatic annotation of seismocardiograms. *IEEE Sens. J.* **2017**, *17*, 2129–2136. [[CrossRef](#)]
41. Yang, C.; Tavassolian, N. Pulse transit time measurement using seismocardiogram, photoplethysmogram, and acoustic recordings: Evaluation and comparison. *IEEE J. Biomed. Health Inform.* **2017**, *22*, 733–740. [[CrossRef](#)] [[PubMed](#)]
42. Paukkunen, M.; Parkkila, P.; Hurmanen, T.; Pänkäälä, M.; Koivisto, T.; Nieminen, T.; Kettunen, R.; Sepponen, R. Beat-by-beat quantification of cardiac cycle events detected from three-dimensional precordial acceleration signals. *IEEE J. Biomed. Health Inform.* **2015**, *20*, 435–439. [[CrossRef](#)] [[PubMed](#)]
43. Lee, J.; McManus, D.D.; Merchant, S.; Chon, K.H. Automatic motion and noise artifact detection in Holter ECG data using empirical mode decomposition and statistical approaches. *IEEE Trans. Biomed. Eng.* **2011**, *59*, 1499–1506.
44. Wu, Z.; Huang, N.E. A study of the characteristics of white noise using the empirical mode decomposition method. *Proc. R. Soc. London. Ser. A Math. Phys. Eng. Sci.* **2004**, *460*, 1597–1611. [[CrossRef](#)]
45. Taebi, A.; Mansy, H. Noise cancellation from vibrocardiographic signals based on the ensemble empirical mode decomposition. *J. Biotechnol. Bioeng.* **2017**, *2*, 00024. [[CrossRef](#)]

46. Chang, K.M.; Liu, S.H. Gaussian noise filtering from ECG by Wiener filter and ensemble empirical mode decomposition. *J. Signal Process. Syst.* **2011**, *64*, 249–264. [[CrossRef](#)]
47. Luu, L.; Dinh, A. Artifact Noise Removal Techniques on Seismocardiogram Using Two Tri-Axial Accelerometers. *Sensors* **2018**, *18*, 1067. [[CrossRef](#)] [[PubMed](#)]
48. Khosrow-Khavar, F.; Tavakolian, K.; Blaber, A.P.; Zanetti, J.M.; Fazel-Rezai, R.; Menon, C. Automatic annotation of seismocardiogram with high-frequency precordial accelerations. *IEEE J. Biomed. Health Inform.* **2014**, *19*, 1428–1434. [[CrossRef](#)] [[PubMed](#)]
49. Shafiq, G.; Tatinati, S.; Veluvolu, K.C. Automatic annotation of peaks in seismocardiogram for systolic time intervals. In Proceedings of the 2016 38th Annual International Conference of the IEEE Engineering in Medicine and Biology Society (EMBC), Orlando, FL, USA, 16–20 August 2016; pp. 2672–2675.
50. Choudhary, T.; Sharma, L.; Bhuyan, M.K. Automatic Detection of Aortic Valve Opening using Seismocardiography in Healthy Individuals. *IEEE J. Biomed. Health Inform.* **2018**, *23*, 1032–1040. [[CrossRef](#)] [[PubMed](#)]
51. Sharma, L.; Dandapat, S.; Mahanta, A. ECG signal denoising using higher order statistics in Wavelet subbands. *Biomed. Signal Process. Control* **2010**, *5*, 214–222. [[CrossRef](#)]
52. Pouymiro, I.R.; Cordova, E.V.; Perez, F.E.V. Robust detection of AO and IM points in the seismocardiogram using CWT. *IEEE Lat. Am. Trans.* **2016**, *14*, 4468–4473.
53. Khosrow-Khavar, F.; Tavakolian, K.; Blaber, A.; Menon, C. Automatic and robust delineation of the fiducial points of the seismocardiogram signal for noninvasive estimation of cardiac time intervals. *IEEE Trans. Biomed. Eng.* **2016**, *64*, 1701–1710. [[CrossRef](#)]
54. Thakkar, H.K.; Sahoo, P.K. Towards Automatic and Fast Annotation of Seismocardiogram Signals Using Machine Learning. *IEEE Sens. J.* **2020**, *20*, 2578–2589. [[CrossRef](#)]
55. Lin, W.Y.; Chou, W.C.; Chang, P.C.; Chou, C.C.; Wen, M.S.; Ho, M.Y.; Lee, W.C.; Hsieh, M.J.; Lin, C.C.; Tsai, T.H.; et al. Identification of location specific feature points in a cardiac cycle using a novel seismocardiogram spectrum system. *IEEE J. Biomed. Health Inform.* **2016**, *22*, 442–449. [[CrossRef](#)]
56. Sorensen, K.; Schmidt, S.E.; Jensen, A.S.; Sogaard, P.; Struijk, J.J. Definition of Fiducial Points in the Normal Seismocardiogram. *Sci. Rep.* **2018**, *8*, 15455. [[CrossRef](#)]
57. Fadil, R.; Aarotale, P.; Hoffmann, B.; Khosrow-Khavar, F.; Xiao, Z.G.; Akhbardeh, A.; Tavakolian, K. Temporal Changes of Fiducial Seismocardiogram Points Due to Different Sensor Placements on the Chest. In Proceedings of the 2020 Computing in Cardiology, Rimini, Italy, 13–16 September 2020; pp. 1–4. [[CrossRef](#)]
58. Jähne-Raden, N.; Gütschleg, H.; Wolf, M.C.; Sigg, S.; Kulau, U. Seismocardiography on Infants and Kids. In Proceedings of the 2020 Computing in Cardiology, Rimini, Italy, 13–16 September 2020; pp. 1–4. [[CrossRef](#)]
59. Chen, C.H.; Lin, W.Y.; Lee, M.Y. The Applications of K-means Clustering and Dynamic Time Warping Average in Seismocardiography Template Generation. In Proceedings of the 2020 IEEE International Conference on Systems, Man, and Cybernetics (SMC), Toronto, ON, Canada, 11–14 October 2020; pp. 1000–1007. [[CrossRef](#)]
60. Sørensen, K.; Poulsen, M.K.; Karbing, D.S.; Søgaard, P.; Struijk, J.J.; Schmidt, S.E. A Clinical Method for Estimation of VO₂max Using Seismocardiography. *Int. J. Sport. Med.* **2020**, *41*, 661–668. [[CrossRef](#)]
61. Yu, S.; Liu, S. A novel adaptive recursive least squares filter to remove the motion artifact in seismocardiography. *Sensors* **2020**, *20*, 1596. [[CrossRef](#)]
62. Morra, S.; Gauthey, A.; Hossein, A.; Rabineau, J.; Racape, J.; Gorlier, D.; Migeotte, P.F.; Le Polain De Waroux, J.B.; Van De Borne, P. Influence of sympathetic activation on myocardial contractility measured with ballistocardiography and seismocardiography during sustained end-expiratory apnea. *Am. J. Physiol.-Regul. Integr. Comp. Physiol.* **2020**, *319*, R497–R506. [[CrossRef](#)]
63. Shandhi, M.M.H.; Fan, J.; Heller, J.A.; Etemadi, M.; Inan, O.; Klein, L. Non-invasive seismocardiography can accurately track changes in pulmonary artery pressures during vasodilator challenge at the time of right heart catheterization. *J. Am. Coll. Cardiol.* **2020**, *75*, 2075–2075. [[CrossRef](#)]
64. Zia, J.; Kimball, J.; Hersek, S.; Shandhi, M.M.H.; Semiz, B.; Inan, O.T. A Unified Framework for Quality Indexing and Classification of Seismocardiogram Signals. *IEEE J. Biomed. Health Inform.* **2020**, *24*, 1080–1092. [[CrossRef](#)] [[PubMed](#)]
65. Hersek, S.; Semiz, B.; Shandhi, M.M.H.; Orlandic, L.; Inan, O.T. A Globalized Model for Mapping Wearable Seismocardiogram Signals to Whole-Body Ballistocardiogram Signals Based on Deep Learning. *IEEE J. Biomed. Health Inform.* **2020**, *24*, 1296–1309. [[CrossRef](#)]
66. Coconcelli, F.; Mora, N.; Matrella, G.; Ciampolini, P. High-Accuracy, Unsupervised Annotation of Seismocardiogram Traces for Heart Rate Monitoring. *IEEE Trans. Instrum. Meas.* **2020**, *69*, 6372–6380. [[CrossRef](#)]
67. Ha, U.; Assana, S.; Adib, F. Contactless Seismocardiography via Deep Learning Radars. In Proceedings of the 26th Annual International Conference on Mobile Computing and Networking. Association for Computing Machinery, MobiCom'20, London, UK, 21–25 September 2020. [[CrossRef](#)]
68. Newman, N.; Gilman, S.; Burdumy, M.; Yimen, M.; Lattouf, O. A Novel Tool for Patient Data Management in the ICU—Ensuring Timely and Accurate Vital Data Exchange Among ICU Team Members. *Int. J. Med. Inform.* **2020**, *144*, 104291. [[CrossRef](#)] [[PubMed](#)]
69. Xia, Z.; Shandhi, M.M.H.; Li, Y.; Inan, O.; Zhang, Y. The delineation of fiducial points for non-contact radar seismocardiogram signals without concurrent ecg. *IEEE J. Biomed. Health Inform.* **2020**, *25*, 1031–1040. [[CrossRef](#)] [[PubMed](#)]

70. Choudhary, T.; Bhuyan, M.K.; Sharma, L.N. Delineation and Analysis of Seismocardiographic Systole and Diastole Profiles. *IEEE Trans. Instrum. Meas.* **2021**, *70*, 1–8. [[CrossRef](#)]
71. Lin, D.J.; Kimball, J.; Zia, J.S.; Ganti, V.G.; Inan, O. Reducing the Impact of External Vibrations on Fiducial Point Detection in Seismocardiogram Signals. *IEEE Trans. Biomed. Eng.* **2021**. [[CrossRef](#)]
72. Choudhary, T.; Das, M.; Sharma, L.; Bhuyan, M. Analyzing seismocardiographic approach for heart rate variability measurement. *Biomed. Signal Process. Control* **2021**, *68*, 102793. [[CrossRef](#)]
73. Hossein, A.; Rabineau, J.; Gorlier, D.; Del Rio, J.I.J.; van de Borne, P.; Migeotte, P.F.; Nonclercq, A. Kinocardiography Derived from Ballistocardiography and Seismocardiography Shows High Repeatability in Healthy Subjects. *Sensors* **2021**, *21*, 815. [[CrossRef](#)] [[PubMed](#)]
74. Morra, S.; Pitisci, L.; Su, F.; Hossein, A.; Rabineau, J.; Racape, J.; Gorlier, D.; Herpain, A.; Migeotte, P.F.; Creteur, J.; et al. Quantification of Cardiac Kinetic Energy and Its Changes During Transmural Myocardial Infarction Assessed by Multi-Dimensional Seismocardiography. *Front. Cardiovasc. Med.* **2021**, *8*, 120. [[CrossRef](#)]
75. Morra, S.; Hossein, A.; Rabineau, J.; Gorlier, D.; Racape, J.; Migeotte, P.F.; Van De Borne, P. Assessment of left ventricular twist by 3D ballistocardiography and seismocardiography compared with 2D STI echocardiography in a context of enhanced inotropism in healthy subjects. *Sci. Rep.* **2021**, *11*, 683. [[CrossRef](#)] [[PubMed](#)]
76. Eyvazi Hesar, M.; Khan, D.; Seyedsadrkhani, N.S.; Ingebrandt, S. Contactless, Battery-free, and Stretchable Wearable for Continuous Recording of Seismocardiograms. *ACS Appl. Electron. Mater.* **2021**, *3*, 11–20. [[CrossRef](#)]
77. Maiorana, E.; Massaroni, C. Biometric Recognition based on Heart-Induced Chest Vibrations. In Proceedings of the 2021 IEEE International Workshop on Biometrics and Forensics (IWBF), Rome, Italy, 6–7 May 2021; pp. 1–6. [[CrossRef](#)]
78. Inan, O.T.; Baran Pouyan, M.; Javaid, A.Q.; Dowling, S.; Etemadi, M.; Dorier, A.; Heller, J.A.; Bicen, A.O.; Roy, S.; De Marco, T.; et al. Novel wearable seismocardiography and machine learning algorithms can assess clinical status of heart failure patients. *Circ. Heart Fail.* **2018**, *11*, e004313. [[CrossRef](#)] [[PubMed](#)]
79. Shandhi, M.M.H.; Fan, J.; Heller, J.A.; Etemadi, M.; Inan, O.T.; Klein, L. Seismocardiography and machine learning algorithms to assess clinical status of patients with heart failure in cardiopulmonary exercise testing. *J. Card. Fail.* **2019**, *25*, S64–S65. [[CrossRef](#)]
80. Malcangi, M.; Quan, H.; Vaini, E.; Lombardi, P.; Di Rienzo, M. Evolving fuzzy-neural paradigm applied to the recognition and removal of artefactual beats in continuous seismocardiogram recordings. *Evol. Syst.* **2020**, *11*, 443–452. [[CrossRef](#)]
81. Mora, N.; Cocconcelli, F.; Matrella, G.; Ciampolini, P. Fully Automated Annotation of Seismocardiogram for Noninvasive Vital Sign Measurements. *IEEE Trans. Instrum. Meas.* **2020**, *69*, 1241–1250. [[CrossRef](#)]
82. D’Mello, Y.; Skoric, J.; Xu, S.; Roche, P.J.; Lortie, M.; Gagnon, S.; Plant, D.V. Real-Time Cardiac Beat Detection and Heart Rate Monitoring from Combined Seismocardiography and Gyrocardiography. *Sensors* **2019**, *19*, 3472. [[CrossRef](#)]
83. Rai, D.; Thakkar, H.K.; Rajput, S.S. Performance Characterization of Binary Classifiers for Automatic Annotation of Aortic Valve Opening in Seismocardiogram Signals. In Proceedings of the 2020 9th International Conference on Bioinformatics and Biomedical Science, ICBBS ’20, Xiamen, China, 16–18 October 2020; pp. 77–82. [[CrossRef](#)]
84. Rai, D.; Thakkar, H.K.; Singh, D.; Bathala, H.V. Machine Learning Assisted Automatic Annotation of Isovolumic Movement and Aortic Valve Closure using Seismocardiogram Signals. In Proceedings of the 2020 IEEE 17th India Council International Conference (INDICON), New Delhi, India, 10–13 December 2020; pp. 1–6. [[CrossRef](#)]
85. Zheng, Y.L.; Ding, X.R.; Poon, C.C.Y.; Lo, B.P.L.; Zhang, H.; Zhou, X.L.; Yang, G.Z.; Zhao, N.; Zhang, Y.T. Unobtrusive sensing and wearable devices for health informatics. *IEEE Trans. Biomed. Eng.* **2014**, *61*, 1538–1554. [[CrossRef](#)]
86. Weissler, A.M.; Harris, W.S.; Schoenfeld, C.D. Systolic time intervals in heart failure in man. *Circulation* **1968**, *37*, 149–159. [[CrossRef](#)] [[PubMed](#)]
87. Paiva, R.; Carvalho, P.; Couceiro, R.; Henriques, J.; Antunes, M.; Quintal, I.; Muehlsteff, J. Beat-to-beat systolic time-interval measurement from heart sounds and ECG. *Physiol. Meas.* **2012**, *33*, 177. [[CrossRef](#)] [[PubMed](#)]
88. Javaid, A.Q.; Fesmire, N.F.; Weitnauer, M.A.; Inan, O.T. Towards robust estimation of systolic time intervals using head-to-foot and dorso-ventral components of sternal acceleration signals. In Proceedings of the 2015 IEEE 12th international conference on wearable and implantable body sensor networks (BSN), Cambridge, MA, USA, 9–12 June 2015; pp. 1–5.
89. Kh Dehkordi, P.; Khosrow-Khavar, F.; Di Rienzo, M.; Inan, O.T.; Schmidt, S.E.; Blaber, A.; Sørensen, K.; Struijk, J.J.; Zakeri, V.; Lombardi, P.; et al. Comparison of Different Methods for Estimating Cardiac Timings: A Comprehensive Multimodal Echocardiography Investigation. *Front. Physiol.* **2019**, *10*, 1057. [[CrossRef](#)] [[PubMed](#)]
90. Korzeniowska-Kubacka, I.; Kuśmierczyk-Droszcz, B.; Bilińska, M.; Dobraszkievicz-Wasilewska, B.; Mazurek, K.; Piotrowicz, R. Seismocardiography—a non-invasive method of assessing systolic and diastolic left ventricular function in ischaemic heart disease. *Cardiol. J.* **2006**, *13*, 319–325.
91. Tavakolian, K.; Khosrow-Khavar, F.; Kajbafzadeh, B.; Marzencki, M.; Rohani, S.; Kaminska, B.; Menon, C. Seismocardiographic adjustment of diastolic timed vibrations. In Proceedings of the 2012 Annual International Conference of the IEEE Engineering in Medicine and Biology Society, San Diego, CA, USA, 28 August–1 September 2012; pp. 3797–3800.
92. Ashouri, H.; Hersek, S.; Inan, O.T. Universal pre ejection period estimation using seismocardiography: Quantifying the effects of sensor placement and regression algorithms. *IEEE Sens. J.* **2017**, *18*, 1665–1674. [[CrossRef](#)]
93. Shandhi, M.M.H.; Semiz, B.; Hersek, S.; Goller, N.; Ayazi, F.; Inan, O. Performance Analysis of Gyroscope and Accelerometer Sensors for Seismocardiography-Based Wearable Pre-Ejection Period Estimation. *IEEE J. Biomed. Health Inform.* **2019**, *23*, 2365–2374. [[CrossRef](#)] [[PubMed](#)]

94. Tadi, M.J.; Koivisto, T.; Pänkäälä, M.; Paasio, A.; Knuutila, T.; Teräs, M.; Hänninen, P. A new algorithm for segmentation of cardiac quiescent phases and cardiac time intervals using seismocardiography. In *Sixth International Conference on Graphic and Image Processing (ICGIP 2014)*; International Society for Optics and Photonics: Bellingham, WA, USA, 2015; Volume 9443, p. 94432K.
95. Rivas-Gotz, C.; Khoury, D.S.; Manolios, M.; Rao, L.; Kopelen, H.A.; Nagueh, S.F. Time interval between onset of mitral inflow and onset of early diastolic velocity by tissue Doppler: A novel index of left ventricular relaxation: experimental studies and clinical application. *J. Am. Coll. Cardiol.* **2003**, *42*, 1463–1470. [[CrossRef](#)]
96. Garrod, A.H. On some points connected with the circulation of the blood, arrived at from a study of the sphygmograph-trace. *Proc. R. Soc. Lond.* **1875**, *23*, 140–151.
97. Chapman, P.M. Abstract of the Goulstonian Lectures on the Physics of the Circulation: Delivered before the Royal College of Physicians. *Br. Med. J.* **1894**, *1*, 511. [[CrossRef](#)]
98. Bowen, W.P. Changes in heart-rate, blood-pressure, and duration of systole resulting from bicycling. *Am. J. Physiol.-Leg. Content* **1904**, *11*, 59–77. [[CrossRef](#)]
99. Bruser, C.; Diesel, J.; Zink, M.D.; Winter, S.; Schauerte, P.; Leonhardt, S. Automatic detection of atrial fibrillation in cardiac vibration signals. *IEEE J. Biomed. Health Inform.* **2012**, *17*, 162–171. [[CrossRef](#)]
100. Hurnanen, T.; Lehtonen, E.; Tadi, M.J.; Kuusela, T.; Kiviniemi, T.; Saraste, A.; Vasankari, T.; Airaksinen, J.; Koivisto, T.; Pänkäälä, M. Automated detection of atrial fibrillation based on time–frequency analysis of seismocardiograms. *IEEE J. Biomed. Health Inform.* **2016**, *21*, 1233–1241. [[CrossRef](#)]
101. Lahdenoja, O.; Hurnanen, T.; Iftikhar, Z.; Nieminen, S.; Knuutila, T.; Saraste, A.; Kiviniemi, T.; Vasankari, T.; Airaksinen, J.; Pänkäälä, M.; et al. Atrial fibrillation detection via accelerometer and gyroscope of a smartphone. *IEEE J. Biomed. Health Inform.* **2017**, *22*, 108–118. [[CrossRef](#)] [[PubMed](#)]
102. Tadi, M.J.; Mehrang, S.; Kaisti, M.; Lahdenoja, O.; Hurnanen, T.; Jaakkola, J.; Jaakkola, S.; Vasankari, T.; Kiviniemi, T.; Airaksinen, J.; et al. Comprehensive analysis of cardiogenic vibrations for automated detection of atrial fibrillation using smartphone mechanocardiograms. *IEEE Sens. J.* **2018**, *19*, 2230–2242. [[CrossRef](#)]
103. Elliott, J.; Belen, M.K.; Mainardi, L.; Rodriguez Matas, J.F. A Comparison of Regional Classification Strategies Implemented for the Population Based Approach to Modelling Atrial Fibrillation. *Mathematics* **2021**, *9*, 1686. [[CrossRef](#)]
104. Cervigón, R.; Moreno, J.; Millet, J.; Pérez-Villacastín, J.; Castells, F. Pulmonary Vein Activity Organization to Determine Atrial Fibrillation Recurrence: Preliminary Data from a Pilot Study. *Mathematics* **2020**, *8*, 1813. [[CrossRef](#)]
105. Yao, J.; Tridandapani, S.; Wick, C.A.; Bhatti, P.T. Seismocardiography-based cardiac computed tomography gating using patient-specific template identification and detection. *IEEE J. Transl. Eng. Health Med.* **2017**, *5*, 1–14. [[CrossRef](#)]
106. Yao, J.; Tridandapani, S.; Auffermann, W.; Wick, C.; Bhatti, P. An adaptive seismocardiography (SCG)-ECG multimodal framework for cardiac gating using artificial neural networks. *IEEE J. Transl. Eng. Health Med.* **2018**, *6*, 1–11. [[CrossRef](#)]
107. Wick, C.A.; Su, J.J.; McClellan, J.H.; Brand, O.; Bhatti, P.T.; Buice, A.L.; Stillman, A.E.; Tang, X.; Tridandapani, S. A system for seismocardiography-based identification of quiescent heart phases: Implications for cardiac imaging. *IEEE Trans. Inf. Technol. Biomed.* **2012**, *16*, 869–877. [[CrossRef](#)]
108. Wick, C.A.; Inan, O.T.; McClellan, J.H.; Tridandapani, S. Seismocardiography-based detection of cardiac quiescence. *IEEE Trans. Biomed. Eng.* **2015**, *62*, 2025–2032. [[CrossRef](#)] [[PubMed](#)]
109. Tadi, M.J.; Lehtonen, E.; Hurnanen, T.; Koskinen, J.; Eriksson, J.; Pänkäälä, M.; Teräs, M.; Koivisto, T. A real-time approach for heart rate monitoring using a Hilbert transform in seismocardiograms. *Physiol. Meas.* **2016**, *37*, 1885. [[CrossRef](#)]
110. Wahlstrom, J.; Skog, I.; Handel, P.; Khosrow-Khavar, F.; Tavakolian, K.; Stein, P.K.; Nehorai, A. A hidden markov model for seismocardiography. *IEEE Trans. Biomed. Eng.* **2017**, *64*, 2361–2372. [[CrossRef](#)]
111. Taebi, A.; Bomar, A.J.; Sandler, R.H.; Mansy, H.A. Heart Rate Monitoring During Different Lung Volume Phases Using Seismocardiography. In Proceedings of the SoutheastCon 2018, St. Petersburg, FL, USA, 19–22 April 2018; pp. 1–5.
112. Lee, H.; Lee, H.; Whang, M. An enhanced method to estimate heart rate from seismocardiography via ensemble averaging of body movements at six degrees of freedom. *Sensors* **2018**, *18*, 238. [[CrossRef](#)] [[PubMed](#)]
113. Siecinski, S.; Tkacz, E.J.; Kostka, P.S. Comparison of HRV indices obtained from ECG and SCG signals from CEBS database. *Biomed. Eng. Online* **2019**, *18*, 69. [[CrossRef](#)] [[PubMed](#)]
114. Charlier, P.; Cabon, M.; Herman, C.; Benouna, F.; Logier, R.; Houfflin-Debarge, V.; Jeanne, M.; De Jonckheere, J. Comparison of multiple cardiac signal acquisition technologies for heart rate variability analysis. *J. Clin. Monit. Comput.* **2019**, *34*, 743–752. [[CrossRef](#)]
115. Mora, N.; Cocconcelli, F.; Matrella, G.; Ciampolini, P. Detection and Analysis of Heartbeats in Seismocardiogram Signals. *Sensors* **2020**, *20*, 1670. [[CrossRef](#)] [[PubMed](#)]
116. Lin, Y.D.; Jhou, Y.F. Estimation of heart rate and respiratory rate from the seismocardiogram under resting state. *Biomed. Signal Process. Control* **2020**, *57*, 101779. [[CrossRef](#)]
117. Sיעיński, S.; Kostka, P.S.; Tkacz, E.J. Heart Rate Variability Analysis on Electrocardiograms, Seismocardiograms and Gyrocardiograms on Healthy Volunteers. *Sensors* **2020**, *20*, 4522. [[CrossRef](#)]
118. Korzeniowska-Kubacka, I.; Bilińska, M.; Piotrowicz, R. Usefulness of seismocardiography for the diagnosis of ischemia in patients with coronary artery disease. *Ann. Noninvasive Electrocardiol.* **2005**, *10*, 281–287. [[CrossRef](#)]
119. Becker, M.; Roehl, A.; Siekmann, U.; Koch, A.; de la Fuente, M.; Roissant, R.; Radermacher, K.; Marx, N.; Hein, M. Simplified detection of myocardial ischemia by seismocardiography. *Herz* **2014**, *39*, 586–592. [[CrossRef](#)]

120. Zanetti, J.M.; Salerno, D.M. Seismocardiography: A technique for recording precordial acceleration. In Proceedings of the Computer-Based Medical Systems Proceedings of the Fourth Annual IEEE Symposium, Baltimore, MD, USA, 12–14 May 1991; pp. 4–9.
121. Koch, A.; McCormack, P.; Schwanecke, A.; Schnoor, P.; Buslaps, C.; Tetzlaff, K.; Rieckert, H. Noninvasive myocardial contractility monitoring with seismocardiography during simulated dives. *Undersea Hyperb. Med.* **2003**, *30*, 19–28. [[PubMed](#)]
122. Tavakolian, K.; Portacio, G.; Tamddondoust, N.R.; Jahns, G.; Ngai, B.; Dumont, G.A.; Blaber, A.P. Myocardial contractility: A seismocardiography approach. In Proceedings of the 2012 Annual International Conference of the IEEE Engineering in Medicine and Biology Society, San Diego, CA, USA, 28 August–1 September 2012; pp. 3801–3804.
123. Verma, A.K.; Fazel-Rezai, R.; Blaber, A.; Tavakolian, K. Pulse transit time extraction from seismocardiogram and its relationship with pulse pressure. In Proceedings of the 2015 Computing in Cardiology Conference (CinC), Nice, France, 6–9 September 2015; pp. 37–40.
124. Yang, C.; Tavassolian, N. Pulse transit time measurement using seismocardiogram and in-ear acoustic sensor. In Proceedings of the 2016 IEEE Biomedical Circuits and Systems Conference (BioCAS), Shanghai, China, 17–19 October 2016; pp. 188–191.
125. Pandia, K.; Inan, O.T.; Kovacs, G.T.; Giovangrandi, L. Extracting respiratory information from seismocardiogram signals acquired on the chest using a miniature accelerometer. *Physiol. Meas.* **2012**, *33*, 1643. [[CrossRef](#)]
126. Pandia, K.; Inan, O.T.; Kovacs, G.T. A frequency domain analysis of respiratory variations in the seismocardiogram signal. In Proceedings of the 2013 35th Annual International Conference of the IEEE Engineering in Medicine and Biology Society (EMBC), Osaka, Japan, 3–7 July 2013; pp. 6881–6884.
127. Zakeri, V.; Akhbardeh, A.; Alamdari, N.; Fazel-Rezai, R.; Paukkunen, M.; Tavakolian, K. Analyzing seismocardiogram cycles to identify the respiratory phases. *IEEE Trans. Biomed. Eng.* **2016**, *64*, 1786–1792. [[CrossRef](#)] [[PubMed](#)]
128. Yang, C.; Antoine, C.; Young, B.K.; Tavassolian, N. A Pilot Study on Fetal Heart Rate Extraction from Wearable Abdominal Inertial Sensors. *IEEE Sens. J.* **2019**, *19*, 10773–10781. [[CrossRef](#)]
129. Smith, V.; Arunthavanathan, S.; Nair, A.; Ansermet, D.; da Silva Costa, F.; Wallace, E.M. A systematic review of cardiac time intervals utilising non-invasive fetal electrocardiogram in normal fetuses. *BMC Pregnancy Childbirth* **2018**, *18*, 370. [[CrossRef](#)] [[PubMed](#)]
130. Landreani, F.; Faini, A.; Martin-Yebra, A.; Morri, M.; Parati, G.; Caiani, E.G. Assessment of Ultra-Short Heart Variability Indices Derived by Smartphone Accelerometers for Stress Detection. *Sensors* **2019**, *19*, 3729. [[CrossRef](#)]
131. Jerosch-Herold, M.; Zanetti, J.; Merkle, H.; Poliac, L.; Huang, H.; Mansoor, A.; Zhao, F.; Wilke, N. The seismocardiogram as magnetic-field-compatible alternative to the electrocardiogram for cardiac stress monitoring. *Int. J. Card. Imaging* **1999**, *15*, 523–531. [[CrossRef](#)]
132. Tavakolian, K.; Dumont, G.A.; Houlton, G.; Blaber, A.P. Precordial vibrations provide noninvasive detection of early-stage hemorrhage. *Shock* **2014**, *41*, 91–96. [[CrossRef](#)]
133. Johnson, E.M.; Heller, J.A.; Vicente, F.G.; Sarnari, R.; Gordon, D.; McCarthy, P.M.; Barker, A.J.; Etemadi, M.; Markl, M. Detecting Aortic Valve-Induced Abnormal Flow with Seismocardiography and Cardiac MRI. *Ann. Biomed. Eng.* **2020**; pp. 1–14. [[CrossRef](#)]
134. Suresh, P.; Narayanan, N.; Pranav, C.V.; Vijayaraghavan, V. End-to-End Deep Learning for Reliable Cardiac Activity Monitoring using Seismocardiograms. *arXiv* **2020**, arXiv:2010.05662.
135. Shandhi, M.M.H.; Aras, M.; Wynn, S.; Fan, J.; Heller, J.A.; Etemadi, M.; Klein, L.; Inan, O.T. Cardiac Function Monitoring for Patients Undergoing Cancer Treatments Using Wearable Seismocardiography: A Proof-of-Concept Study. In Proceedings of the 2020 42nd Annual International Conference of the IEEE Engineering in Medicine & Biology Society (EMBC), Montreal, QC, Canada, 20–24 July 2020; pp. 4075–4078.
136. Pravdin, S.; Kononov, P.; Dierckx, H.; Solovyova, O.; Panfilov, A.V. Drift of Scroll Waves in a Mathematical Model of a Heterogeneous Human Heart Left Ventricle. *Mathematics* **2020**, *8*, 776. [[CrossRef](#)]
137. Ramírez, W.A.; Gizzi, A.; Sack, K.L.; Filippi, S.; Guccione, J.M.; Hurtado, D.E. On the Role of Ionic Modeling on the Signature of Cardiac Arrhythmias for Healthy and Diseased Hearts. *Mathematics* **2020**, *8*, 2242. [[CrossRef](#)]
138. Yanase, J.; Triantaphyllou, E. The seven key challenges for the future of computer-aided diagnosis in medicine. *Int. J. Med. Inform.* **2019**, *129*, 413–422. [[CrossRef](#)] [[PubMed](#)]